1. INTRODUCTION

1.1. Background to research

1.1.1. General Background

The Atomic Energy Corporation (AEC) has been involved in research into the development of processes for the production of different metallic oxides (mainly ZrO_2, Al_2O_3 and SiO_2) for several years in the so-called Metox Programme.

A lot of development work has been completed and this work has culminated in a pilot plant with a production capacity of approximately 200 metric tons/year for the production of different grades of zirconia (ZrO_2) and silica (SiO_2). The aim of this pilot plant is the evaluation of the developed technology on a large enough scale to facilitate the generation of parameters and data for the design of a commercial scale plant (on a scale of 10 000 tons/year total ZrO_2 production).

Two grades of zirconia can be produced by this plant: a high grade zirconia (ca. 99.3% total ZrO_2 and HfO_2) and a very high grade zirconia (ca. 99.8% total ZrO_2 and HfO_2). The high grade zirconia is produced via the so-called 'dry route' and the very high grade via the so-called 'wet route'. For a discussion on zirconium and hafnium chemistry, see Section 2.1.3.

The developed processes revolve around the use of hydrofluoric acid (HF) for the main reactions. The AEC is strategically positioned to take advantage of this dangerous and reactive acid because of the core competency developed in the area of HF handling and processing. This core competency developed as a result of the use of HF in the enrichment process for uranium and also because the AEC has an HF manufacturing plant on site.

Four patents are owned by the Atomic Energy Corporation regarding the HF processes, including international patents on both the 'wet route' and 'dry route' manufacture of zirconia.

1.1.2. Plasma dissociation

The prime raw material for both the wet and dry production routes is zircon sand ($ZrSiO_4$). This mineral is mined from beach sand in appropriate areas and beneficiated via physical separation methods. The main South African companies producing this mineral are Namakwa Sands and Richards Bay Minerals (RBM).

The zircon is highly unreactive and has to be activated by some means to make it suitable for further processing.

Dissociation of the zircon crystal structure by exposing the zircon to high temperatures is well-known in literature. At the AEC the activation is achieved by exposing the zircon to effective particle temperatures in the region of 1800 °C in a non-transfer arc plasma reactor, which dissociates the zircon according to the following reaction:

$$ZrSiO_4(s) \xrightarrow[1800^\circ C]{} ZrO_2.SiO_2(s) \qquad \textbf{(Eq 1.1)}$$

The product solids consists of particles containing submicron crystalline particulates (or crystallites) of zirconia in an amorphous structure of silica. This product is called Plasma Dissociated Zircon (PDZ) and is chemically much more reactive than zircon.

The PDZ in itself is a possible product from the process because of its superior opacifying properties and resulting application in the opacifier industry. It also shows promising results as a component in the manufacture of pigments.

1.1.3. The 'wet route'

Step 1: Dissolution of PDZ

The 'wet route' earned its name because the first step in the processing of the PDZ is the dissolution with HF in aqueous medium according to the following reaction:

$$ZrO_2.SiO_2(s) + 12HF(aq) \rightarrow H_2ZrF_6(aq) + H_2SiF_6(aq) + 4H_2O(l) \qquad \textbf{(Eq 1.2)}$$

The product of this process step is a liquid solution of the hydrofluozirconic acid (H_2ZrF_6) and the hydrofluosilicic acid (H_2SiF_6) in a solution of HF in water. This solution is called the 'mother liquor'. Because the reaction is exothermic, heat has to be removed from the solution.

All insoluble impurities are filtered out during this step.

The hydrofluosilicic acid can not exist on its own but only exists in aqueous solutions of HF and water. When it comes into contact with pure water, SiF_4 reacts according to the following reaction[1]:

$$3SiF_4 + 2H_2O \rightarrow SiO_2 + 2H_2SiF_6 \qquad \textbf{(Eq 1.3)}$$

The silica formed in this manner is a viscous gel, which could block up pipelines or cause other problems. Thus any scrubber used for removal of condensables from off-gas must have a residual concentration of HF (not only to prevent the formation of silica, but also to absorb the SiF_4, which is not easily absorbed in water, but absorbs readily as H_2SiF_6 in an aqueous phase when HF is present).

Step 2: Crystallisation of hydrofluozirconic acid

The mother liquor is heated and flash evaporated in a flash chamber. The hydrofluosilicic acid dissociates according to the following reaction:

$$H_2SiF_6(aq) \xrightarrow[heat]{} SiF_4(g) + 2HF(g) \qquad \textbf{(Eq 1.4)}$$

HF and water is also evaporated from the solution and the hydrofluozirconic acid crystallises out in the solution (alternatively the solution can be brought only to saturation point before cooling). The solution is cooled down to maximise yield and the acid crystals are filtered out.

The crystals are then dried in an oven and forms several crystalline structures, the main of which are zirconium tetrafluoride (ZrF_4) and zirconium oxyfluorides ($Zr_xO_yF_z$).

Step 3: Conversion of zirconium compounds to zirconia

The zirconium compound crystals are then treated in a rotary kiln at approximately 600 °C to produce zirconia as follows (main reactions only):

$$\begin{aligned} ZrOF_2(s) + H_2O(g) &\xrightarrow[600°C]{} ZrO_2(s) + 2HF(g) \\ ZrF_4(s) + 2H_2O(g) &\xrightarrow[600°C]{} ZrO_2(s) + 4HF(g) \end{aligned} \qquad \textbf{(Eq 1.5)}$$

The HF is recovered and recycled in the process. The zirconia is the final product of the wet route at a purity of ca. 99.8%.

1.1.4. The 'dry route'

Step 1: Reaction of PDZ with gaseous HF

The dry route also utilises PDZ as its input solid material. A direct gas-solid reaction is carried out to produce zirconia in a fluidized bed reactor at 120 °C according to the following reaction:

$$ZrO_2.SiO_2(s) + 4HF(g) \xrightarrow[120°C]{} ZrO_2(s) + SiF_4(g) + 2H_2O(g) \qquad \textbf{(Eq 1.6)}$$

Because of incomplete conversion of zircon to PDZ in the plasma reactor (approximately 85 to 90% conversion of zircon), incomplete conversion in the fluidized bed reactor (approximately 99% conversion of PDZ) and residual impurities in the zircon sand, the product solids contains several impurities. These impurities have to be removed.

The silicon tetrafluoride (SiF_4) in the off-gas is recovered in a thermal plasma reactor at approximately 1000 °C according to the following reaction:

$$SiF_4(g) + 2H_2O(g) \Leftrightarrow SiO_2(s) + 4HF(g) \qquad \textbf{(Eq 1.7)}$$

The silica produced is a high quality fumed silica and is one of the main products of the integrated process.

The HF is recovered and recycled as reaction gas for the fluidized bed reactor. As a result of this step, there is nearly no waste produced by the dry route, and a very low net input of HF is necessary. The net loss of HF in the process results from adsorbed HF on the fluidized bed and the silica system solid products, and also the formation of some zirconium oxyfluorides during the fluidized bed reaction.

The total amount of fluorides (free and bound) on the product solids from the fluidized bed depends mainly on the exposure time of solids to HF and the gaseous concentration of the HF. Thus there is a direct link between solids conversion and fluoride concentration on the fluidized bed product.

Step 2: Product polishing or beneficiation of fluidized bed product

Because of the porous structure of the product zirconia and the relative hardness of the remaining zircon, a physical separation can be achieved by careful milling of the product in a slurry and a classification step where the slurry is separated according to particle size. The product slurry is then filtered out in a filter press and washed to remove as much of the remaining fluorides as possible.

The resultant product has a purity in excess of 99.3% ZrO_2 and HfO_2.

Step 3: Spray drying of product

As the product polishing is carried out in aqueous medium, the product has to be dried. This is achieved in a spray dryer, which also serves as an agglomerator to produce particles of the desired particle size according to client specifications.

1.1.5. Product applications

As will be illustrated by example, zirconia in its unstabilized and stabilized form, and also the chemicals derived from it, find an abundance of applications in very diverse fields. These applications necessitate the production of zirconia of various grades of purity, depending on the application, and illustrate the need for the development of efficient and cost-effective zirconia production technologies.

1.1.5.1. Unstabilized zirconia

Zirconia is used in a finely dispersed form to enhance the thermal shock resistance of other ceramic materials. For example[2], it is added to alumina (the so-called ZTA or zirconia-toughened alumina[3]) for use in the sliding gate valves which are an integral part of the continuous casting process for steel and for nozzles and stoppers of transfer and holding ladles, with its enhancement of corrosion and thermal shock resistance. It is also used for dispersion hardening of platinum and ruthenium[4].

Zirconium oxide fused with alumina in electric-arc furnaces is used to make alumina-zirconia abrasive grains for use in grinding wheels, coated-abrasive disks, and belts[4]. The addition of zirconia toughens the alumina, reducing brittleness, and resulting in high strength, hardness, and surface crystal sharpness, resulting in fast grinding and long wheel life[5].

Zirconia has application as a catalyst for some reactions[4].

Zirconia is an important raw material for the production of optical glasses (where it is used to increase the refractive index[4]), new abrasives, piezoelectric elements, ceramic capacitors and other electronic devices[6]. For these applications, generally a silica content of less than 0.1% is required[7].

Zirconia is also used to produce pigments of various colours, such as praseodymium-zircon yellow, vanadium-zircon blue and iron-zircon pink[4].

Single-crystal cubic zirconias of high purity are produced as synthetic diamonds[4].

Zirconia is used to coat the surface of titanium oxide pigment particles for some exterior paints. This zirconia coating minimises ultraviolet excitation of the titania, which would interact with the organic paint binder and reduce service life[5].
Zirconia has been used as the pigment of white camouflage paints for use in snow environments in preference to titania, because zirconia more closely simulates snow in the infrared and microwave spectra[5].

Zirconium chemicals such as zirconium sulphate, zirconium carbonate, zirconium oxychloride, etc., are generally manufactured from either baddeleyite or synthetic zirconia, and are used in applications such as: leather tanning, pigment coatings, printing inks, flame-proofing of wool and textiles, and anti-perspirants.

1.1.5.2. Stabilized zirconia

The high melting point (>2700 °C) and the excellent chemical properties (very high resistance to alkalis and acids[5]) of zirconia would suggest its use as a refractory. The monoclinic-tetragonal phase transformation of zirconia at approximately 1100 °C with an accompanying volume change of 3-5% precludes its direct use as a refractory.

This problem with the volume change associated with the phase transformation of zirconia has led to the development of stabilized zirconias, where either the tetragonal or cubic phase is stabilized by the introduction of oxides of mainly Mg, Ca, Y and Ce.

Stabilized or partially stabilized zirconia is used in the refractory industry and also for so-called engineering ceramics, because of its high strength and toughness[6].

Yttria-stabilized zirconia is used to form thermal barrier coatings (TBC) in high heat flux applications such as the Space Shuttle Main Engine (SSME) by NASA[8].

Yttria- or calcia-stabilized zirconias are used as the solid electrolyte in oxygen sensors in automotive and boiler exhausts, and oxygen-content probes for molten copper or iron in smelters[4], because vacancies in the anion lattice at elevated temperatures allow O^{2-} ions to diffuse[5].

Inductively heated yttria-stabilized zirconia cylinders are used as heat sources to melt quartz boules for the drawing of quartz optical fibres[5].

Yttria-stabilized zirconia membranes are used in high-temperature pH sensors (300 °C compared to the 120 °C for the normal glass electrode) and these pH sensors are used in the direct measurement of pH of geothermal brines, of water in nuclear reactors, and in high-temperature corrosion studies[9].

Stabilized zirconia has other diverse applications, such as[4]: ceramic tubing, extrusion dies, ball-milling media, high temperature heating elements, insulating fibres, ceramic diesel engines, and a nonlubricated ball-bearing assembly for use in a space vehicle, also[5]: fishing rod ferrules, knives, unbreakable shirt buttons and golf putter heads, and[2]: hot gas filters and electrolysis diaphragms.

1.1.6. Market background

The main raw material for the production of zirconia is zircon. This mineral is produced as a by-product of the mining of other minerals, generally the titanium-containing minerals rutile, ilmenite[4] and leucoxene[5], and the consumption of zircon in 1997 was approximately 900 000 tonnes[11]. The production of zircon is thus mostly linked to the demand for titanium metal and the paint-market demand for titanium oxide pigment[5].

The direct use of zircon as refractories, foundry sands and opacifiers in glazes for tiles and sanitary wares accounted for 60% of the U.S. consumption and the conversion into other forms of zircon for the remaining 40% in 1984[4].

The utilisation spread for total produced zircon in 1995 was as follows[5]: 35-40% for ceramic glazes and enamels, 30-35% for refractories, 15-20% in foundry use, 8-12% in abrasives, and 8-12% in other uses such as chemicals, metals and alloys, and glass constituents.

Natural zirconia, also known as baddeleyite, is produced mainly at Phalaborwa in South Africa, at a rate of approximately 18 000 tonnes per year (1997). Synthetic zirconia, primarily produced from zircon, was produced at a rate of approximately 20 000 tonnes per year in 1997[10].

The four major producing countries of zirconium minerals were (1996)[5]: Australia 50%, South Africa 25%, United States 10% and the Ukraine 6%. By 1999, South Africa's share of total world zirconium mineral production has risen to 43%, with a production of approximately 395 000 tonnes/year[11].

Zirconia selling prices depend heavily on purity grade, and selling prices in 1993 ranged from $2/kg for low-purity grades of baddeleyite to over $50/kg for high purity stabilized grades[3]. Prices in 1999 are still in the same range[11].

1.2. Thesis objectives

The pilot plant fluidized bed for the gas-solid reaction between the PDZ and HF had to be designed from results generated on a lab scale fluidized bed setup. To achieve this, a reaction kinetic model was necessary that could accurately predict conversion of the PDZ to zirconia for different operating conditions.

UNIVERSITEIT VAN PRETORIA
UNIVERSITY OF PRETORIA
YUNIBESITHI YA PRETORIA

This reaction kinetic model had then to be used for the modelling of a continuous fluidized bed on pilot plant scale to facilitate design of the pilot plant fluidized bed for production of the desired amount and quality of zirconia. It also had to maximise HF consumption efficiency.

The objective of this thesis is the achievement of these aims:

1. **The development of a reliable reaction kinetic model describing the gas-solid reaction between PDZ and HF.**

2. **The incorporation of the reaction kinetic model into a model for a continuous fluidized bed.**

3. **The use of the resulting model for optimisation of PDZ conversion and HF efficiency with the minimum bed load (or solids residence time).**

2. THEORETICAL MODEL DEVELOPMENT

2.1. Literature background and discussion on chemistry

2.1.1. Reaction kinetics

Reaction kinetics is a measure of the *rate* of reaction, as opposed to thermodynamics, which is a measure of the *extent* of reaction possible.

Reaction kinetics plays a very important part in chemical engineering – it is the main tool used for reactor design or sizing. It also makes possible the prediction of the product conversion for a given set of operating variables and a given reactor.

A few basic reactor models exist (such as the batch reactor, the continuously stirred tank reactor (CSTR) and the plug flow reactor (PFR)). These models have been combined and modified to various extents to imitate or model different real systems.

As mentioned in Section 2.3.1.1, a fluidized bed is usually modelled such that the solids are uniformly mixed (CSTR) and the gas flows in plug flow (PFR).

2.1.1.1 Reaction kinetics basics

Generally, the reaction rate of a substance A with substance B can be written as:

$$-r_A = [k(T)][function(C_A, C_B, \ldots)] \qquad \textbf{(Eq 2.1)}$$

When this relationship between the reaction rate and the different variables on the right-hand side of the equation has been determined, it can be used together with the relevant reactor model for reactor design or prediction of reactor performance.

The variable k in Equation 2.1 is called the *reaction rate constant*. Its units can vary, depending on the form of the equation, and it can generally be described as a function of temperature according to the Arrhenius equation:

$$k(T) = A_f e^{-E/R_g T} \qquad \textbf{(Eq 2.2)}$$

The constants in Equation 2.2 (A_f and E) can be determined after the rate equation has been determined by running the reaction at different temperatures and calculating k for each temperature from Equation 2.1 and the experimental results. Alternatively, if it is a well-known reaction, values could be available from literature.

2.1.1.2 Determining the rate-limiting step

Various reaction steps can be identified when looking at a gas-solid reaction:

1. External diffusion of the reactant gas to the particle surface.
2. Internal diffusion of the reactant gas through the solid particle to an active reaction site (porous particles only).

3. Reaction of the reactant with a specific mineral in the particle.
4. Internal diffusion of gaseous reaction products out of the particle (porous particles only).
5. External diffusion of reaction products away from the particle.

For some reactions (mostly catalytic), step 3 can be divided into a further three steps[12]:

3a Adsorption of the reactant onto the solid surface.
3b Reaction on the surface.
3c Desorption of reaction products from solid surface.

Generally, one of the steps named above dominates, and will determine the rate of reaction, although it is possible that there could be a transition from one rate-limiting step to another during the course of a reaction. An example is a reaction with a solid particle where the particle becomes porous over time. It is possible that the reaction could initially be the rate-limiting step, with internal diffusion becoming dominant as the particle becomes more porous.

The development of equations for the above reaction steps can be found in various literature sources. The development of equations for some of the reaction steps for the reaction between PDZ and gaseous HF specifically, is shown in Section 2.2.

The determination of the reaction order of the reaction rate equation with respect to the different reactants, can be done using various rate analysis methods, such as[13]: the *differential method*, the *method of initial rates*, etc. These methods require that experiments be run with each of the reactants in excess (the so-called *method of excess*) during data generation.

When it is not possible to use the method of excess (e.g. how can a large excess of solids in a gas-solid reaction be obtained and the gas concentration as function of time measured at the same time?), the *integral method* can be used. In the integral method, a rate equation is assumed, and the rate constant is determined by integrating the differential equation for the batch system.

The rate constant can be determined by doing a *least-squares analysis* on the equations resulting from the different models. This analysis minimises the sum of the squares of the errors that the model makes in its prediction of data points. In this case the analysis was used to determine the model with the smallest error in predicting conversion rates (after the various rate constants were determined).

This last-mentioned method requires the assumption of a rate model for analysis. Thus a few theoretical models can be proposed and developed, based on experience and experimental evidence, and then these models can be evaluated against experimental data to determine the best fit. This method has been followed for the reactions in this thesis.

2.1.1.3 Solid particle reaction models

Only two of the more relevant solid particle reaction models will be looked at here: the Shrinking Core Model and the Uniform Reaction Model, which represents the two extreme models for gas-solid reactions.

Examples of intermediate models are[13]: the porous-pellet model of Ishida and Wen and the grain model of Sohn and Szekely.

Shrinking Core Model

This model is used when a gas and a solid material reacts and some sort of reaction front advances into the particle. When the reaction products are only gaseous, the whole particle will react away over time.

When one of the reaction products is a solid, or some component of the solid material does not react, the result is a particle with a reaction front or surface that keeps converging on the centre of the particle, leaving an inert porous particle structure or matrix behind.

The Shrinking Core Model can be used assuming different rate-limiting steps. Depending on the rate-limiting steps, some assumptions have to be made. For example, when internal diffusion of the HF to the surface of the shrinking core of PDZ is assumed to be the rate-limiting step, the assumption of equimolar counterdiffusion is made[12]. One of the major assumptions of the Shrinking Core Model is the assumption of spherical particles.

For a particle that becomes porous over time, the particle diameter or size also influences the rate-limiting step. When the particles are very large, the chances that internal diffusion will be rate-limiting is increased. When the particles are very small, the chances for reaction rate as the rate-limiting step is increased.

A quantification method for this effect is proposed by *Fogler*[12], in which a diameter, D*, is determined where the mass transfer and reaction rate resistances are equal:

$$D^* = \frac{2D_e}{k_s} \qquad \textbf{(Eq 2.3)}$$

When $d_p > D^*$ mass transfer is rate-limiting
$d_p < D^*$ reaction rate is rate-limiting

Uniform Reaction Model

In the Uniform Reaction Model, material is assumed to react at equal rate through the whole particle. A prerequisite for this type of reaction is a porous particle to start with and fast diffusion rates, so that reaction rate is the rate-limiting step.

The gaseous reactant is assumed to be present in equal concentrations throughout the particle. For very small particles, the uniform reaction model is usually sufficiently accurate[13].

2.1.2. Fluidized bed basics

2.1.2.1. Hydrodynamic considerations

When a fluid is passed upwards through a bed of particles, and the velocity is continuously increased, distinct changes in the behaviour of the particles can be observed. At first, the bed of particles remain stationary and this is called a *fixed bed.*

With increase in fluid velocity, the bed is seen to expand – the volume fraction of voids is increased. This is called an *expanded bed.*

With a further increase in velocity, the bed reaches a point where all the particles are just suspended by the upward-flowing fluid[13]. The bed is then at the point of *minimum fluidization.* With further increase in velocity, different fluidized behaviours can be observed (depending on the particle and fluid properties), such as *smooth fluidization, bubbling fluidization, slugging* and *turbulent fluidization,* until eventually all particles are blown out of the bed and it becomes a *moving bed.*

A general classification of particles to predict its behaviour when attempting fluidization is the well-known *Geldart* classification[14].

When fluidized, a bed of particulate solids will exhibit similar flow properties to a liquid, in that it will flow to equalise levels and maintain a horizontal surface.

From the above discussion it is clear that there are limits to the fluidization regime in terms of fluid velocity for solid particles. The determination of these limits is one of the first steps in designing a fluidized bed for particular applications.

The **lower limit** of fluid velocity is called the *minimum fluidization velocity.* This is the minimum superficial fluid velocity to facilitate fluidization for a particular bed of solid particles.

Various theoretical equations for the determination of the minimum fluidization velocity exist, such as the one by Kunii & Levenspiel[13]:

$$\frac{1.75}{\varepsilon_{mf}^3 \phi_s} \mathrm{Re}_{p,mf}^2 + \frac{150(1-\varepsilon_{mf})}{\varepsilon_{mf}^3 \phi_s^2} \mathrm{Re}_{p,mf} = Ar$$

$$\mathrm{Re}_{p,mf} = \frac{d_p u_{mf} \rho_g}{\mu} \qquad \textbf{(Eq 2.4)}$$

$$Ar = \frac{d_p^3 \rho_g (\rho_s - \rho_g) g}{\mu^2}$$

The porosity at minimum fluidization (ε_{mf}) is a function of temperature and pressure and should be determined experimentally at the design operating conditions. Although the theoretical equations for determining the minimum fluidization velocity are reasonably accurate, calculations should always be backed up by experimental work.

The **upper limit** on fluid velocity for fluidization is set by the terminal velocity of particles in the bed of solids. Above this velocity, particles will be entrained in the off-gas stream. For design purposes, the smallest particle size that is present in significant numbers should be chosen for this calculation.

The terminal velocity of a free-falling particle is given by[13]:

$$u_t = \left[\frac{4d_p(\rho_s - \rho_g)g}{3\rho_g C_D}\right]^{1/2} \quad \textbf{(Eq 2.5)}$$

where the drag coefficient, C_D, is given by[15]:

$$C_D = \frac{24}{\mathrm{Re}_p}[1 + (8.1716e^{-4.0655\phi_s})\mathrm{Re}_p^{\,0.0964+0.5565\phi_s}] + \frac{73.69(e^{-5.0748\phi_s})\mathrm{Re}_p}{\mathrm{Re}_p + 5.378e^{6.2122\phi_s}} \quad \textbf{(Eq 2.6)}$$

For the assumption of spherical particles, the sphericity (ϕ_s) reduces to 1. The sphericity for a particular type of solids with a particular particle size distribution can be determined experimentally using methods as described by Kunii & Levenspiel[13].

The pressure drop across a bed of particles at minimum fluidization can be estimated by[13]:

$$\Delta P_b = (1 - \varepsilon_{mf})(\rho_s - \rho_g)gh_{mf} \quad \textbf{(Eq 2.7)}$$

2.1.2.2. Bubble models

The bubble models facilitate the prediction of the change in the value of the rate constant for different operating conditions. In this it helps diminish the general scale-up problems associated with fluidized bed design in the past.

The effectiveness of gas-solid contacting in a fluidized bed is of course one of the most important design properties. As the gas moves upward through the bed mostly in bubble form, it can be appreciated that modelling of the bubble behaviour in the fluidized bed is an important part of design.

Various bubble models exist, such as the Davidson model, the Collins & Stewart model, the Jackson model and the Murray model. These bubble models can be incorporated into a flow model that describes hydrodynamic behaviour of the fluidized bed. This flow model is important because it has a significant influence on the effectiveness of gas-solid contacting and thus the kinetics of reaction between gas and solid.

The theoretical derivation of equations for the determination of the effective reaction rate constant in a fluidized bed is quite involved and is treated in detail by Kunii & Levenspiel[13].

For reaction in a small particle bed with all mass transfer resistances taken into account, the overall rate constant is given by[13]:

$$k_f = \left[\gamma_b k_r + \frac{1}{\frac{1}{k_{bc}} + \frac{1}{\gamma_c k_r + \frac{1}{\frac{1}{k_{ce}} + \frac{1}{\gamma_e k_r}}}} \right] \qquad \textbf{(Eq 2.8)}$$

This equation is used to calculate the effective overall reaction rate constant, with hydrodynamic effects in the fluidized bed taken into account.

2.1.2.3. Residence time distributions

The solids behaviour in a fluidized bed is generally modelled as similar to that in a CSTR. The residence time distribution function for solid particles in a single stage fluidized bed is thus given by:

$$E(t) = \frac{1}{\bar{t}} e^{\frac{-t}{\bar{t}}} \qquad \textbf{(Eq 2.9)}$$

The residence time distribution function for a multi-stage reactor:

$$E(t) = \frac{1}{(i-1)!\bar{t}} \left(\frac{t}{\bar{t}} \right)^{i-1} e^{\frac{-t}{\bar{t}}} \qquad \textbf{(Eq 2.10)}$$

From this, the cumulative residence time distribution fraction can be calculated as follows:

$$F(t) = \int_0^t E(t)dt \qquad \textbf{(Eq 2.11)}$$

2.1.2.4. Practical considerations

L-valves

When transferring solids from one stage to the next in a multi-stage fluidized bed externally, it is necessary to create a gas seal between the stages so that gas from the one stage does not short-circuit through the transfer pipe instead of the provided gas outlet.

This solid transporter usually takes the form of a L-valve or J-valve. A typical L-valve is shown in Figure 2.1. It consists of vertical and horizontal pipe sections, with a gas inlet just above the top level of the horizontal section (this was shown to be the optimum position for

the gas inlet by Knowlton & Hirsan[16]). It has no moving mechanical parts, and the solids in the vertical or downcomer section provide the gas seal.

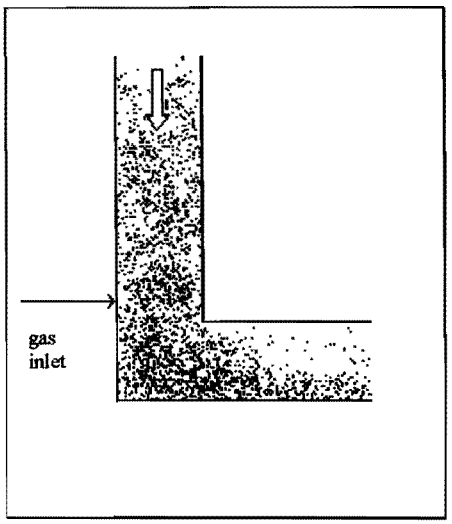

Figure 2.1 Typical L-valve

By controlling the gas flow rate to the gas inlet of the L-valve, the solids flow rate through the L-valve can be controlled. To ensure gas sealing, the solids in the downcomer section must have a certain minimum height. This minimum solids height can be calculated using equations from Knowlton & Hirsan[16]. The minimum downcomer diameter and the minimum length of the horizontal section can be calculated using equations from Picciotti[17].

Distribution plates

Distribution plates can take various forms, such as porous or perforated plates, pipe grids and spargers, etc., as well as bubble caps or tuyeres to prevent solids backflow on shutdown[18]. The specific design depends on the particular application.

The pressure drop over the distributor for a fluidized bed should be designed to be[19]:

$$\frac{\Delta P_d}{\Delta P_b} \geq \left(\frac{h}{h_{mf}} - 1\right)\frac{1}{1-(u_{mf}/u_o)^n} \qquad \textbf{(Eq 2.12)}$$

here n=1 for porous plates and n=2 for perforated plates.

Internal baffles in fluidized beds

Internal baffles can be used for internal staging of fluidized beds where appropriate. This internal staging can effect a large reduction in required reactor solids load for a specified conversion when correctly specified.

The use of internal baffles can largely reduce short-cutting of solids across the bed and ensure a narrower residence time distribution. Internal baffles also promote smaller bubbles in the bed[20].

Transport disengagement height and entrainment

A fluidized bed can usually be divided into two zones: a dense, bubbling phase with a distinct upper level and a more dilute phase that consists of the off-gas with some entrained particles. As the bed height is increased, the particle density in the off-gas decreases until it reaches a constant value. The height at which this particle density becomes constant is called the *transport disengagement height (TDH)* or freeboard (measured from the upper surface of the dense bed)[13].

By designing a fluidized bed to include sufficient freeboard, the entrainment and elutriation of particles in the off-gas stream can be minimised.

The reason for the entrainment is two-fold: very fine particles have terminal velocities lower than the superficial gas velocity through the bed, and some particles are thrown into the freeboard area by bursting bubbles. As these particles lose their kinetic energy, the larger particles return to the bed[18].

Equations for the calculation of the TDH for Geldart A beds (fine, less dense particles) are given by Kunii & Levenspiel[13]. An equation for the prediction of entrainment from a fluidized bed for specific operating conditions and Geldart A beds, which includes provision for the TDH, is given by Perry[18]. The use of these equations should always be backed up by experimental work, if possible.

2.1.3. Some aspects of zirconium chemistry

2.1.3.1 Zirconium and hafnium

Zirconium and hafnium always occur together in nature, usually with a hafnium content in the range of 1-3% of total hafnium and zirconium content. Because of the very similar physical and chemical behaviour of the two metals, it is generally not necessary to separate the two materials[3, 4, 5, 21].

It was also historically difficult to obtain separation because of the similar properties. Interest in separation grew because of the observation that zirconium has a very low thermal neutron cross-section (0.18 barns), while hafnium has a high thermal neutron cross-section (105 barns)[22].

This led to the application of zirconium metal or alloys as reactor core components in thermal nuclear reactors and this application is the only commercially important one that requires separation of the two metals. In fact, the hafnium-free zirconium metal producing industry was launched as an integral part of the nuclear power industry in the late 1940's and early 1950's[5].

Separation of zirconium and hafnium is today routinely done via multistage counter-current liquid-liquid extraction[4].

Because of the co-existence of zirconium and hafnium in natural compounds, and the very similar physical and chemical behaviour, the separation of these two metals is unnecessary except for the nuclear industry (as stated above), and thus, whenever compounds of

zirconium are mentioned in this thesis, THE UNDERSTANDING IS THAT IT INCLUDES A HAFNIUM CONTENT OF APPROXIMATELY 2 m/m % OF TOTAL (Zr + Hf) CONTENT.

2.1.3.2 Zirconium and hydrogen fluoride

The number of chemical interactions between zirconium and HF are large, and some disagreement over the composition of some compounds still persist. The chemical reactions introduced in Section 1.1 are simplifications of the real situation.

For example, hydrofluozirconic acid (H_2ZrF_6) usually exists associated with some crystal water, the molar ratio of which depends on the prior processing and processing temperatures. The main compound of these is $H_2ZrF_6.2H_2O$.

Other fluozirconic acids that could exist in aqueous medium are[21]: $H_3Zr_2F_{11}.5H_2O$, $H_2ZrOHF_5.2H_2O$ and $H_2ZrF_6.H_2O$.

Overfluorination of dissociated zircon with gaseous HF (as could happen in the fluidized bed reactor) and excessive reaction temperatures (above approximately 140 °C) lead to the formation of zirconium oxyfluoride ($ZrOF_2$). This $ZrOF_2$ can readily be converted to zirconia by treatment with steam at a temperature of approximately 320 °C:

$$ZrOF_2 + H_2O \xrightarrow[320°C]{} ZrO_2 + 2HF \qquad \textbf{(Eq 2.13)}$$

A good summary of the chemistry of the zirconium-tetrafluoride-hydrate system is given in the Journal of Inorganic Nuclear Chemistry[23].

2.2. Kinetic models

2.2.1. General

As discussed previously, the reaction under examination is the gas-solid reaction between PDZ and hydrofluoric acid, or the main reaction in the fluidized bed reactor of the dry route.

It must be kept in mind that, because of incomplete conversion, the feed solids actually consist of a mixture of PDZ and undissociated zircon, the latter of which will not participate in the reaction. This undissociated zircon will thus remain in the solids phase, co-existing with DPDZ (or zirconia) in the product particles.

The species in the reaction will be represented by the following letters:

$ZrO_2.SiO_2(s)$	+	4HF(g)	→	$ZrO_2(s)$	+	$SiF_4(g)$	+	$2H_2O(g)$
Zircon (PDZ)	+	hydrofluoric acid	→	zirconia (DPDZ)	+	silicon tetrafluoride	+	water
A	+	4B	→	C	+	D	+	2E

The following definitions are of importance:

X_A = Conversion of PDZ to DPDZ = $(C_{Ao} - C_A)/C_{Ao}$ (does NOT include undissociated zircon contained in feed solids) []

W = Solids mass (INCLUDING undissociated zircon) [kg]

2.2.2. Reaction as rate-limiting step

2.2.2.1. Mass as solids driving force

If solids mass is taken as the solids driving force for reaction and it is assumed that the reaction is first order in regards to HF concentration, then the following rate equation can be defined for the reaction:

$$-r_A = kWC_B \qquad \textbf{(Eq 2.14)}$$

Here it is important to correctly define the mass of solids present at any time. For this, it is first necessary to define the initial concentration of PDZ (PLEASE NOTE - these calculations are performed for illustration purposes and for a batch operation):

$$C_{Ao} = \frac{YW_o}{V_{bed}M_r(PDZ)} = \frac{YW_o}{\frac{W_0}{\rho_b} * \frac{L_{mf}}{L_m} * M_r(PDZ)} = \frac{Y\rho_b L_m}{L_{mf}M_r(PDZ)} \qquad \textbf{(Eq 2.15)}$$

Now the mass of solids present at any time can be defined as:

Mass of solids = Initial mass of solids - mass of silica reacted away

$$\begin{aligned} W &= W_0 - C_{Ao}X_A M_r(SiO_2)V_{bed} \\ \therefore W &= W_o\left[1 - X_A Y\frac{M_r(SiO_2)}{M_r(PDZ)}\right] \\ \therefore W &= W_o(1 - cX_A) \\ \left[c = Y\frac{M_r(SiO_2)}{M_r(PDZ)}\right] & \end{aligned} \qquad \textbf{(Eq 2.16)}$$

The bulk density of the solids as function of time is given by:

$$\rho_{b,t} = \rho_b(1 - cX_A(t)) \qquad \textbf{(Eq 2.17)}$$

Substituting for W in Equation 2.14:

$$\begin{aligned} -r_A &= k_{ws}(1 - cX_A)C_B \\ \left[k_{ws} = kW_o\right] & \end{aligned} \qquad \textbf{(Eq 2.18)}$$

As an alternative to the above model and Equation 2.18, the mass of PDZ in the solids instead of the mass of solids can be used as solids driving force for the reaction (which is a more realistic representation of reality). The following equations result:

$$\rho_{PDZ,b} = \rho_b Y(1 - X_A)$$
$$-r_A = kW_{PDZ}C_B = k\rho_{PDZ,b}V_{bed}C_B \qquad \textbf{(Eq 2.19)}$$
$$\therefore -r_A = k\rho_b Y V_{bed}(1 - X_A)C_B$$

With substitution for the rate constant:

$$-r_A = k_{wp}(1 - X_A)C_B$$
$$\left[k_{wp} = k\rho_b Y V_{bed}\right] \qquad \textbf{(Eq 2.20)}$$

2.2.2.2. Surface area as solids driving force

Here the external surface area of PDZ is taken as solids driving force for reaction, with a shrinking core of PDZ in a porous matrix of zirconia.

The model is based on experimental photographic evidence (obtained by scanning electron microscopy or SEM) and collates with the general physical property differences between the feed solids and the product, such as the fact that the particle size distributions of the feed solids (consisting mostly of PDZ) and the product solids (consisting mostly of zirconia) are generally similar (average particle size in the region of 110 microns and no large reduction in particle sizes).

Because particle sizes remain approximately constant, and the silica is reacted away, the assumption of a porous particle product is reasonable.

A few concepts are of importance here:

- The diameter (and thus external surface area) of the core of PDZ is a variable of time.
- The solids density of the core of PDZ in the particle remains constant (NOT the bulk density).
- The volume and mass of PDZ are variables of time.
- The total number of particles remains constant throughout the reaction.

With these concepts in mind, a model can now be built. The reaction rate is a function of the HF gas concentration, as well as the total exposed surface of PDZ according to the shrinking core model. The reaction rate equation then looks as follows:

$$-r_A = k_s A_{sc} C_B \qquad \textbf{(Eq 2.21)}$$

Careful definition of the surface area is now necessary. The total external surface area of the particles of PDZ in a given mass of feed solids at zero time is given by:

$$A_{sc,o} = aW_{PDZ\,0} \qquad \textbf{(Eq 2.22)}$$

The relationship between the diameter of the shrinking core of PDZ and conversion for a single particle of feed solids:

$$\begin{aligned} m_{PDZ} &\propto (1 - X_A) \\ m_{PDZ} &\propto V_{PDZ} \\ V_{PDZ} &\propto d_{sc}^3 \\ \therefore d_{sc} &\propto (1 - X_A)^{\frac{1}{3}} \\ d_{sc} &= d_{sco}(1 - X_A)^{\frac{1}{3}} \end{aligned} \qquad \textbf{(Eq 2.23)}$$

In the above equation, d_{sco} represents the initial diameter of the shrinking core of PDZ in a particle. As this is the same as the particle diameter d_p, d_p can be substituted for d_{sco} in the above equation.

The external surface area of the shrinking core of PDZ can now be related to conversion as follows (from Equations 2.22 and 2.23):

$$\begin{aligned} A_{sc} &\propto d_{sc}^2 \\ \therefore A_{sc} &\propto (1 - X_A)^{\frac{2}{3}} \\ A_{sc} &= aW_{PDZo}(1 - X_A)^{\frac{2}{3}} \end{aligned} \qquad \textbf{(Eq 2.24)}$$

The definition of the specific surface area of PDZ:

$$a = \frac{6}{\rho_{PDZ} d_s} \qquad \textbf{(Eq 2.25)}$$

Thus, by inserting Equations 2.25 into Equation 2.24, the total surface area of PDZ for a given mass of solids is given by:

$$A_{sc} = \frac{6W_{PDZo}}{d_s \rho_{PDZ}}(1 - X_A)^{\frac{2}{3}} \qquad \textbf{(Eq 2.26)}$$

Substituting this definition for the total surface area of PDZ into the rate equation, Equation 2.21, gives:

$$-r_A = \frac{6k_s W_{PDZo}}{d_s \rho_{PDZ}}(1-X_A)^{\frac{2}{3}} C_B$$

$$-r_A^{'} = b(1-X_A)^{\frac{2}{3}} C_B \qquad \textbf{(Eq 2.27)}$$

$$\left[b = \frac{6k_s W_{PDZo}}{d_s \rho_{PDZ} h} \right]$$

The parameter b is constant for isothermal operation and can be defined in terms of more readily definable parameters:

$$W_{PDZo} = YW_o$$

$$\therefore b = \frac{6k_s YW_o}{d_s \rho_{PDZ} h} \qquad \textbf{(Eq 2.28)}$$

2.2.3. External diffusion as rate-limiting step

If external diffusion of HF to the particle surface is assumed to be the rate-limiting step, mass transfer of the HF to the particle surface must be analysed.

Several equations for the prediction of the mass transfer coefficient exist, such as the Thoenes-Kramers equation for flow through a packed bed[12], or the equation from Kunii-Levenspiel for flow through a fluidized bed[13].
A general equation for external mass transfer[24]:

$$\varepsilon_{mf} j_m = 2.06 \,\mathrm{Re}_D^{-0.575} \phi_s \qquad \textbf{(Eq 2.29)}$$

where the Colburn j factor for mass transfer, j_m, is given by:

$$j_m = \frac{Sh_D}{\mathrm{Re}_D \, Sc^{\frac{1}{3}}} \qquad \textbf{(Eq 2.30)}$$

From these equations:

$$Sh_D = (2.06 \mathrm{Re}_D^{0.425} \, Sc^{\frac{1}{3}}) \Big/ \varepsilon_{mf} \qquad \textbf{(Eq 2.31)}$$

UNIVERSITEIT VAN PRETORIA
UNIVERSITY OF PRETORIA
YUNIBESITHI YA PRETORIA

The general reaction rate equation for external diffusion of HF as rate-limiting step:

$$-r_A = A_{ext} k_m (C_B - C_{Bs}) \qquad \textbf{(Eq 2.32)}$$

Because reaction and internal diffusion take place faster than external diffusion, the HF concentration at the external particle surface (C_{Bs}) can be approximated as zero, and so the reaction rate equation (Equation 2.32) becomes:

$$-r_A = A_{ext} k_m C_B \qquad \textbf{(Eq 2.33)}$$

where k_m is calculated using Equation 2.30.

The external surface area, A_{ext} , can be calculated as follows (where A_{ext} = the number of particles multiplied by the external surface area for the area-equivalent average particle size):

$$A_{ext} = N_p \times \pi \overline{d_{pa}^2} \qquad \textbf{(Eq 2.34)}$$

where the number of particles, N_p , is given by the mass of solids divided by the average particle mass:

$$N_p = \frac{W}{\overline{m_p}} \qquad \textbf{(Eq 2.35)}$$

The average particle mass is given by (again the average particle diameter is the mass average particle diameter):

$$\overline{m_p} = \frac{1}{6} \pi \overline{d_{pm}^3} \rho_s \qquad \textbf{(Eq 2.36)}$$

Combining these equations (Equations 2.34, 2.35 and 2.36) gives an expression for the external surface area in terms of known quantities:

$$A_{ext} = \frac{6W \overline{d_{pa}^2}}{\overline{d_{pm}^3} \rho_s} \qquad \textbf{(Eq 2.37)}$$

Substituting this equation (Equation 2.37) into Equation 2.33 gives the following rate equation:

$$-r_A = A_{ext} k_m C_B = \frac{6W \overline{d_{pa}^2}}{\overline{d_{pm}^3} \rho_s} k_m C_B \qquad \textbf{(Eq 2.38)}$$

$$-r_A = k_{ED} W C_B$$

u14738405
b14436000

where the composite rate constant, k_{ED}, is given by:

$$k_{ED} = \frac{6k_m \overline{d_{pa}^2}}{\overline{d_{pm}^3}\rho_s} \qquad \textbf{(Eq 2.39)}$$

Thus, with substitution for W from Equation 2.16, Equation 2.38 can be written as:

$$-r_A = k_{ED} W_o (1 - cX_A) C_B \qquad \textbf{(Eq 2.40)}$$

2.2.4. Internal diffusion as rate-limiting step

For internal diffusion of HF to a reaction site as the rate-limiting step, it is important to correctly define the effective diffusivity[12]:

$$D_e = \frac{D_A \varepsilon_p \sigma}{\tau} \qquad \textbf{(Eq 2.41)}$$

here σ = constriction factor []
τ = tortuosity []
ε_p = particle porosity []
D_A = gas diffusivity [m^2/s]

For typical values of the above parameters, the following relationship exist[12]:

$$D_e \approx 0.1 D_A \qquad \textbf{(Eq 2.42)}$$

For diffusion and reaction in a solid particle and gases in dilute concentration, the following differential equation applies[12]:

$$\frac{d^2 C_B}{dr^2} + \frac{2}{r}\left(\frac{dC_B}{dr}\right) - \frac{k_{surf} A_{int}}{D_e} C_B = 0 \qquad \textbf{(Eq 2.43)}$$

where k_{surf} = the reaction rate constant per unit surface area

Equation 2.43 can be simplified by substituting the following dimensionless variables[12]:

$$\varphi = \frac{C_B}{C_{Bs}}$$
$$\lambda = \frac{r}{R} \qquad \textbf{(Eq 2.44)}$$

For a first-order reaction with regards to HF, Equation 2.43 now becomes[12]:

$$\frac{d^2\varphi}{d\lambda^2} + \frac{2}{\lambda}\left(\frac{d\varphi}{d\lambda}\right) - \Phi_1^2\varphi$$
$$\Phi_1^2 = \frac{k_{surf} R^2 S_a \rho_s}{D_e} \qquad \textbf{(Eq 2.45)}$$

The solution to the above differential equation is given by[12]:

$$\varphi = \frac{1}{\lambda}\left(\frac{\sinh\Phi_1\lambda}{\sinh\lambda_1}\right) \qquad \textbf{(Eq 2.46)}$$

An internal effectivity factor, η, can be defined that is an indication of the relative importance of diffusion and reaction as rate-limiting steps, and can have a value of between 0 and 1.

For the above case[12]:

$$\eta = \frac{3}{\Phi_1^2}\left(\Phi_1 \coth\Phi_1 - 1\right) \qquad \textbf{(Eq 2.47)}$$

Thus, for first order reaction with regards to HF and internal diffusion the rate-limiting step, the reaction rate equation now looks as follows:

$$-r_A = \frac{3}{R}\sqrt{\frac{D_e S_a k_{surf}}{\rho_s}} C_B W$$
$$-r_A = k_{ID} W C_B \qquad \textbf{(Eq 2.48)}$$
$$\left[k_{ID} = \frac{3}{R}\sqrt{\frac{D_e S_a k_{surf}}{\rho_s}}\right]$$

Thus, with substitution for W from Equation 2.16, Equation 2.48 becomes:

$$-r_A = k_{ID} W_o (1 - cX_A) C_B \qquad \textbf{(Eq 2.49)}$$

2.2.5. Comparison of model rate equations

From the discussion on bubble models in Section 2.1.2.2, it was seen that the bubble models facilitate the prediction of the change in the value of the rate constant for different operating conditions. The incorporation of a bubble model into the rate equation is achieved by the various methods as discussed in Section 2.1.2.2. This section does not look at the bubble models as such, but whenever a rate constant is used in an equation, the implication is that it represents the composite rate constant as calculated by the Kunii-Levenspiel model (Eq 2.8).

If the five rate equations are compared as follows, some interesting observations can be made:

1. Reaction as rate-limiting step, with solids mass as solids driving force, Equation 2.18:

$$-r_A = k_{ws}(1-cX_A)C_B$$
$$\left[k_{ws} = kW_o\right]$$

2. Reaction as rate-limiting step, with PDZ mass as solids driving force, Equation 2.20:

$$-r_A = k_{wp}(1-X_A)C_B$$
$$\left[k_{wp} = k\rho_b Y V_{bed}\right]$$

3. Reaction as rate-limiting step, with PDZ surface area as solids driving force, Equation 2.27:

$$-r_A = bh(1-X_A)^{\frac{2}{3}}C_B$$
$$\left[b = \frac{6k_s Y W_{PDZo}}{d_s \rho_{PDZ} h}\right]$$

4. External diffusion as rate-limiting step, Equation 2.40:

$$-r_A = k_{ED} W_o (1-cX_A)C_B$$
$$\left[k_{ED} = \frac{6k_m \overline{d_{pa}^2}}{\overline{d_{pm}^3}\rho_s}\right]$$

5. Internal diffusion as rate-limiting step, Equation 2.49:

$$-r_A = k_{ID} W_o (1-cX_A)C_B$$
$$\left[k_{ID} = \frac{3}{R}\sqrt{\frac{D_e S_a k_{surf}}{\rho_s}}\right]$$

The following observations can be made:

- Rate equations 1, 4 and 5 are very similar, the difference lying in the definition and thus calculation of the overall rate constant.
- Four of the five equations have a dependence on $(1\text{-}X_A)$ in various forms (two in the form $(1\text{-}cX_A)$, while the fifth, equation 3, has a dependence on $(1\text{-}X_A)^{2/3}$. This would suggest that the four equations would yield similar results for calculation of the conversion as function of time.

2.3. *Application of model to fluidized beds*

2.3.1. Single -stage fluidized bed

Detailed derivation of the model for the single-stage semi-continuous fluidized bed (with a batch bed load and a continuous feed of gas) is only done for the model using the rate equation developed in Section 2.2.2.2. The models for the other rate equations can be derived in a similar manner and only the results are shown in Section 2.3.1.2.

2.3.1.1 Detailed development of model using shrinking core rate equation

The following assumptions are made in the derivation of this model (these are standard assumptions for a simplified fluidized bed model[25, 26]):

1. Plug flow for the gas mixture with constant concentration over the bed area.
2. Uniform mixing of the solids over the bed volume.
3. The superficial gas velocity stays constant over the bed height (but not between stages).

The third assumption can be shown to be reasonable using a simple example. For a 40 mole % HF, 60 mole % steam gas feed (typical), and a 50% conversion in a single stage:

z_{B0}	= 0.4	[]
δ	= -0.25	[]
ΔX	= 0.5	[]

Then change in volumetric gas flow rate is given by:

$$\Delta Q = \varepsilon.\Delta X = z_{B0}.\delta.\Delta X = 0.4*-0.25*0.5 = -0.05$$

Thus 50% reaction in a single stage only causes a 5% change in volumetric gas flow rate. The assumption of no gas volume change in the bed is thus reasonable.

Taking a mole balance for HF over a differential reactor volume (where y is bed height measured from the distribution plate):

IN - OUT + GENERATED= STORED

$$A_d u_o C_B(y) - A_d u_o C_B(y+dy) - 4b(1-X_A)^{\frac{2}{3}} C_B dy = 0 \qquad \textbf{(Eq 2.50)}$$

Rearranging gives:

$$\frac{dC_B}{dy} = -\frac{4b}{A_d u_o}(1-X_A)^{\frac{2}{3}} C_B \qquad \textbf{(Eq 2.51)}$$

With conversion constant over the bed height, Equation 2.51 can be integrated as follows:

$$\int_{C_{Bo}}^{C_B} \frac{dC_B}{C_B} = -\frac{4b}{A_d u_o}(1-X_A)^{\frac{2}{3}} \int_0^h dy$$

$$\therefore C_B = C_{Bo} e^{-n(t)y}$$

$$n(t) = \frac{4b}{A_d u_o} f(t) \qquad \textbf{(Eq 2.52)}$$

$$f(t) = (1-X_A(t))^{\frac{2}{3}}$$

This equation gives the HF concentration at any bed height as a function of conversion, which is in turn a function of reaction time.

Because the solids conversion is constant over the bed height at any specific point in time (due to the uniform mixing assumption), an average HF concentration over the bed height can be found by integrating the HF concentration over the bed height:

$$\overline{C_B} = \frac{1}{h}\int_0^h C_B dy \qquad \textbf{(Eq 2.53)}$$

With some manipulation the following equation for the average HF concentration over the bed height results:

$$\overline{C_B} = \frac{p}{f}(1-e^{-qf})$$

$$p = \frac{C_{Bo} d_s \rho_{PDZ} A_d u_o}{24 k_s Y W_o} \qquad \textbf{(Eq 2.54)}$$

$$q = \frac{C_{Bo}}{p}$$

Taking a mole balance for PDZ over the reactor volume:

IN - OUT + GENERATED= STORED

$$0 - 0 + r_A' h = \frac{dN_A}{dt}$$

$$\frac{dN_A}{dt} = -b(1-X_A)^{\frac{2}{3}} \overline{C_B} h \qquad \textbf{(Eq 2.55)}$$

The number of moles of PDZ (N_A) in the reactor can be defined as follows:

$$N_A = N_{Ao}(1-X_A)$$

$$\therefore dN_A = -N_{Ao} dX_A \qquad \textbf{(Eq 2.56)}$$

Through combination of Equations 2.54, 2.55 and 2.56:

$$\frac{dX_A}{dt} = \frac{bh}{N_{Ao}}(1-X_A)^{\frac{2}{3}} \frac{p}{(1-X_A)^{\frac{2}{3}}}\left[1-e^{-qf}\right]$$

$$\frac{dX_A}{dt} = \frac{bph}{N_{Ao}}\left[1-e^{-q(1-X_A)^{\frac{2}{3}}}\right] \qquad \textbf{(Eq 2.57)}$$

Equation 2.57 can be integrated to give conversion of PDZ as function of time by doing a rearrangement as follows:

$$\int_0^{X_A} \frac{dX_A}{\left[1-e^{-q(1-X_A)^{\frac{2}{3}}}\right]} = \frac{bph}{N_{Ao}} \int_0^t dt \qquad \textbf{(Eq 2.58)}$$

This equation can be solved using numerical integration to calculate conversion as function of time.

2.3.1.2 Summary of model results for other rate equations

The four other models produce integral equations that can be solved analytically, although the final equation for PDZ conversion as function of time is implicit and must be solved iteratively or by computer. It is hard not to notice the similarities in the results for the four models, as mentioned in Section 2.2.5.

Derivation of the equation for the first model below is shown in Appendix A. Equations for the other models can be derived in similar manner.

Reaction as rate-limiting step, with solids mass as solids driving force:

$$X_A - \frac{1}{sc}\ln\left[\frac{1-e^{-s(1-cX_A)}}{1-e^{-s}}\right] = \frac{C_{B0}A_d u_0}{4hN_{A0}}t$$

where **(Eq 2.59)**

$$s = \frac{4k_{ws}h}{A_d u_0}$$

Reaction as rate-limiting step, with PDZ mass as solids driving force:

$$X_A - \frac{1}{s}\ln\left[\frac{1-e^{-s(1-X_A)}}{1-e^{-s}}\right] = \frac{C_{B0}A_d u_0}{4hN_{A0}}t$$

where **(Eq 2.60)**

$$s = \frac{4k_{wp}h}{A_d u_0}$$

External diffusion as rate-limiting step:

$$X_A - \frac{1}{sc}\ln\left[\frac{1-e^{-s(1-cX_A)}}{1-e^{-s}}\right] = \frac{C_{B0}A_d u_0}{4hW_0 N_{A0}}t$$

where **(Eq 2.61)**

$$s = \frac{4k_{ED}W_0 h}{A_d u_0}$$

Internal diffusion as rate-limiting step:

$$X_A - \frac{1}{sc}\ln\left[\frac{1-e^{-s(1-cX_A)}}{1-e^{-s}}\right] = \frac{C_{B0}A_d u_0}{4hW_0 N_{A0}}t$$

where **(Eq 2.62)**

$$s = \frac{4k_{ID}W_0 h}{A_d u_0}$$

2.3.2. Multi-stage continuous fluidized bed

As the solid phase in a fluidized bed generally behaves as a CSTR (Continuously Stirred Tank Reactor), it can be appreciated that large reductions in reactor sizes for equal conversion can be gained by multi-staging.

A few different reactor configurations were investigated to try to strike a balance between minimising total reactor bed volume for the required PDZ conversion and simultaneously maximising HF consumption efficiency. The two main continuous models are developed here.

NOTE: Development of the continuous fluidized bed models are only done for the model with reaction as rate-limiting step and the PDZ surface area as solids driving force, because this model yielded the best correlation with experimental results, as shown in Section 4.1.1.

2.3.2.1 Three stage counter-current flow fluidized bed reactor

Figure 2.2 shows a diagram of the three stage counter-current flow fluidized bed reactor for modelling purposes and indicates notation.

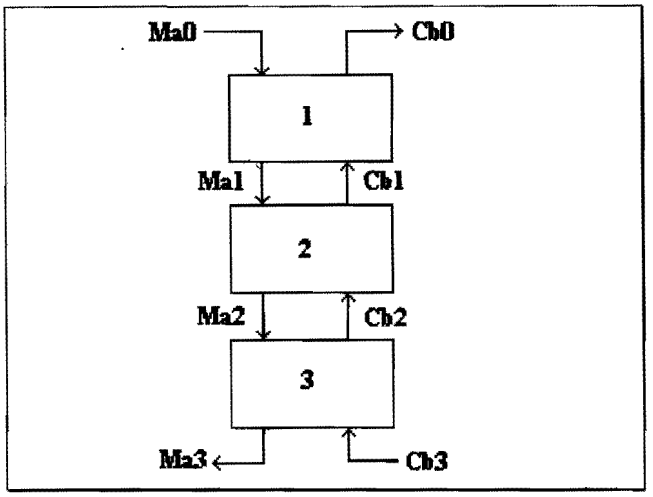

Figure 2.2 Three stage countercurrent fluidized bed reactor

NOTE: Solids load in stages are not necessarily equal.

Using the reaction rate equation and setting up a PDZ mole balance over stage 1 (where M_A denotes the molar flow rate of PDZ in kmol/s):

IN - OUT + GENERATED = STORED

$$M_{A0} - M_{A1} - bh_1(1 - X_{A1})^{\frac{2}{3}}\overline{C_{B1}} = 0$$

where **(Eq 2.63)**

$$h_1 = h_{10}\frac{(1-\varepsilon_m)}{(1-\varepsilon_{mf})}$$

By defining a dimensionless flow rate, the equation can be simplified as follows:

$$\gamma_i = \frac{M_{Ai}}{M_{A0}}$$

then **(Eq 2.64)**

$$\gamma_1 + \frac{bh_1}{M_{A0}}\gamma_1^{\frac{2}{3}}\overline{C_{B1}} = 1$$

The equations for the other two stages can be derived in a similar manner:

$$\gamma_2 + \frac{bh_2}{N_{A0}}\gamma_2^{\frac{2}{3}}\overline{C_{B2}} = \gamma_1$$

$$\gamma_3 + \frac{bh_3}{N_{A0}}\gamma_3^{\frac{2}{3}}\overline{C_{B3}} = \gamma_2 \quad \textbf{(Eq 2.65)}$$

The HF concentration after every stage can be calculated directly from Equation 2.52.

This model then gives six simultaneous equations (three for conversion and three for HF concentration) with six unknowns – γ_1, γ_2, γ_3, C_{B1}, C_{B2} and C_{B3} – which can be solved using a spreadsheet or mathematical computer package.

2.3.2.2 Multi-stage counter-/cross-current flow fluidized bed reactor

Figure 2.3 shows a diagram for a combination of counter- and cross-current flows in a multi-stage fluidized bed reactor. This type of combination was found to be much more effective than the normal counter-current configuration, as was shown by the results of the computer modelling of these configurations (see Section 4.2.2.1).

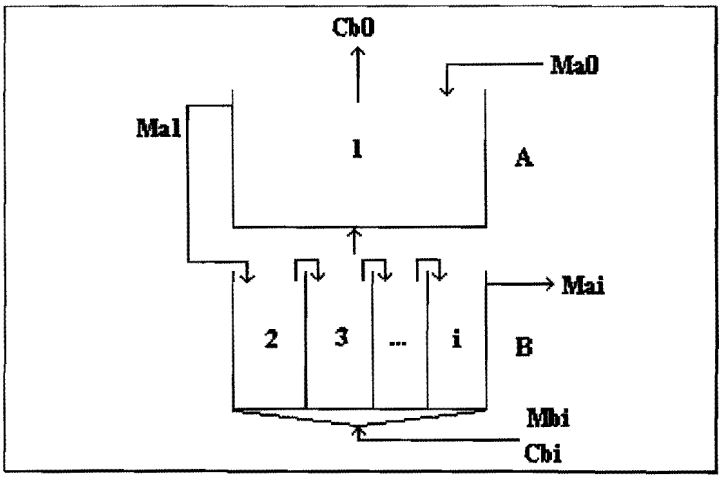

Figure 2.3 Cross-/countercurrent fluidized bed reactor

NOTE: Solids loads in the various stages are not necessarily equal, but the total cross-sectional area of stage 1 is equal to the total cross-sectional area of the subsequent stages.

The total cross-sectional area of stages A and B are equal:

$$A_{d(A)} = A_{d(B)} \qquad \textbf{(Eq 2.66)}$$

The change in HF mole flow rate for each subsection of stage B is calculated as follows:

$$M_{Bi} = g_i M_{Bin} - 4M_{A0}(X_i - X_{i-1})$$

where **(Eq 2.67)**

$$g_i = \frac{A_{di}}{A_{dtot}}$$

The change in volumetric gas flow rate for each subsection of stage B is calculated as shown:

$$Q_i = g_i Q_{in}(1 + \varepsilon_B(X_i - X_{i-1}))\frac{P_{out}}{P_{in}}$$

where **(Eq 2.68)**

$$\varepsilon_B = z_{B0}\delta$$

The outlet HF concentration in each of the substages of stage B:

$$C_{Bi} = \frac{M_{Bi}}{Q_i} \qquad \textbf{(Eq 2.69)}$$

With the assumption of complete gas mixing after stage B, the total mixed outlet HF concentration from stage B is: (see Section 2.3.3 for the assumption of no gas mixing)

$$C_{B1} = \frac{\sum_{2}^{i} M_{Bi}}{\sum_{2}^{i} Q_i} = \frac{M_{B1}}{Q_1} \qquad \textbf{(Eq 2.70)}$$

The outlet HF concentration for stage 1 (or A) can be calculated directly from Equation 2.52. An identical equation to the one for stage 1 of the three-stage model can be derived by taking a PDZ mole balance over stage 1:

$$\gamma_1 + \frac{bh_1}{M_{A0}} \gamma_1^{\frac{2}{3}} \overline{C_{B1}} = 1 \qquad \textbf{(Eq 2.71)}$$

Similar equations result for the substages of stage B:

$$\gamma_i + \frac{bh_i}{M_{A0}} \gamma_i^{\frac{2}{3}} \overline{C_{Bi}} = \gamma_{i-1} \qquad \textbf{(Eq 2.72)}$$

This model results in 2i equations with 2i unknowns (γ_1 to γ_i and C_{B0} to C_{Bi-1}), that can be solved using a spreadsheet or mathematical computer package.

2.3.3. Influence of gas mixing

The model developed in section 2.3.2.2 assumed total gas mixing between the main stages A and B. Thus the gas entering stage A was modelled as a gas stream with uniform concentration. This model thus assumed enough height, diffusion and turbulence for total mixing.

The other extreme is no gas mixing between stages. By modelling this extreme as well, two limits to the real situation are obtained. To model no gas mixing between the main stages A and B, stage A is divided into a corresponding number of substages as stage B, each with its own entering gas concentration. The entering gas concentrations for stage A are obtained from Equation 2.52.

Now the equations for the substages of stage A can be developed in a similar manner as those for stage B in Section 2.3.2.2.

The change in HF mole flow rate for each subsection of stage A is calculated as follows:

$$M_{Bi} = g_i M_{Bi,in} - 4M_{A0}(X_i - X_{i-1})$$

where **(Eq 2.73)**

$$g_i = \frac{A_{di}}{A_{dtot}}$$

The change in volumetric gas flow rate for each subsection of stage A is calculated as shown:

$$Q_i = g_i Q_{in}(1 + \varepsilon_B(X_i - X_{i-1}))\frac{P_{out}}{P_{in}}$$

where **(Eq 2.74)**

$$\varepsilon_B = z_{B0}\delta$$

The outlet HF concentration in each of the substages of stage A:

$$C_{Bi} = \frac{M_{Bi}}{Q_i} \quad \textbf{(Eq 2.75)}$$

Similarly to the previous section, taking a mole balance for PDZ over each of the substages yields the following equations:

$$\gamma_1 + \frac{bh_1}{M_{A0}}\gamma_1^{\frac{2}{3}}\overline{C_{B1}} = 1$$

$$\gamma_i + \frac{bh_i}{M_{A0}}\gamma_i^{\frac{2}{3}}\overline{C_{Bi}} = \gamma_{i-1} \quad \textbf{(Eq 2.76)}$$

This model results in 2i equations with 2i unknowns (γ_1 to γ_i and C_{B0} to C_{Bi-1}), that can be solved using a spreadsheet or mathematical computer package. (Of course, in staying with the notation as set out in Figure 2.3 for the total system with the i-1 substages for stage B, the total number of equations and unknowns are now 4(i-1), where i is the actual number of stages and 2(i-1) is the number of stages for the no gas mixing model.)

2.4. Design of pilot plant fluidized bed reactor

Various factors came into play with the design of the pilot plant fluidized bed setup. A few of them are looked at here briefly.

2.4.1. Effect of mass loss on gas flow distribution

For the cross-current staging (as shown in Figure 2.3), it was realised that the loss in particle mass coupled with the different conversions in the cross-current stages, will lead to different pressure drops, which will lead to a redistribution of gas flows.

In other words, the stage with the highest conversion will have the lowest pressure drop for the same flow rate, and thus its flow rate will increase until the pressure drop is the same as for the other stages.

The effect of this redistribution of gas flows on solids conversion was investigated and results are given in Section 4.2.1.4. The calculations were done by utilising the hydrodynamic equations for bed behaviour from Section 2.1.2.1. The typical conversion in each of the substages was obtained from the reaction kinetic model.

2.4.2. Design of internal baffles

When inserting vertical internal baffles in a fluidized bed for cross-current staging, a very important aspect is the intermixing of solids between stages. As solids are thrown up into the off-gas by bursting bubbles, these solids can fall into the next / previous stage if the bubble bursts close to a baffle.

When this interstage mixing rate increases above the solids feed rate to the first stage, the positive effect of staging is diminished, until the bed behaves like a single stage without internals.

For this reason the pilot plant bed was designed with internal baffles that contain narrow horizontal slits for solids flow to the next stage, to try to minimise interstage mixing (see Figure 2.4). These slits are not the full width of the bed, but less than half the bed width. They are also arranged in a staggered configuration to minimise shortcutting of particles through a stage (see top view of reactor in Figure 2.4).

This baffle design was tested in the full-scale fluidized bed model and it was found to provide satisfactory flow of solids through the beds, while minimising interstage mixing.

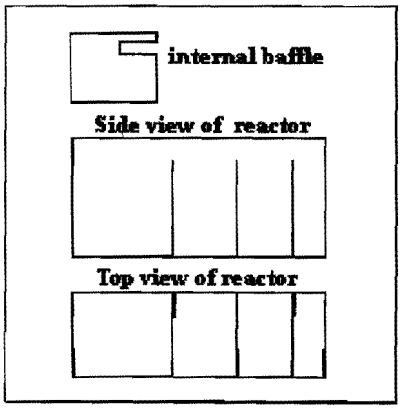

Figure 2.4. Internal baffles in second main reactor stage

2.4.3. The use of distribution pipes

Two full-scale fluidized bed models with the same dimensions as the pilot plant fluidized bed was built: a perspex bed with distributor plate and internal heat exchange tubes, and a mild steel bed with internal baffles. These models were used to observe and evaluate the hydrodynamic behaviour of the solids in the fluidized bed design.

The full-scale models were built because the pilot plant bed was going to be manufactured from Monel (a very expensive metal alloy of nickel and copper) and any design mistakes would have been very costly.

On running the full-scale models, it was noticed that some of the holes in the distributor plates got blocked every time the air flow to the beds was switched off and switched on again later. This was because of particles getting stuck in the holes.

The problem was that, when the holes are made smaller, no reduction in blockages are observed. When the holes are made larger, sand falls through when gas flow is switched off, and fewer holes can be used (for equal pressure drop), which decreases the effectiveness of gas distribution over the whole cross-sectional area of the bed.

Alternative configurations were investigated and it was decided to use distribution pipes. Bubble caps would not have been a viable choice because of the construction cost (bearing in mind that Monel or Teflon would have had to be used) and the complicated bed internals that result from a bubble cap design.

Distribution pipes were designed with central distributors and the pipes running along the length of the rectangular bed (the same orientation as the heat exchange pipes – see Figure 2.5). The holes in the pipes are situated at a 45 degree angle from the vertical, on the underside of the pipes. The angle is there to ensure that the bubbles flow upwards around the desired side of the distribution pipe.

The distribution pipe design was found to be a great success, with no more blockages and the configuration making it possible to switch off gas flow to the bed without having to drain it first. Low maintenance is also important because of the fact that the process gas is toxic, making elaborate safety precautions necessary whenever the reactor is opened.

2.4.4. Bubble break-up by heat-exchange tubes

Because of the fact that the reaction rate is greatly influenced by the effectiveness of gas-solid contact, and large gas bubbles are detrimental to this efficiency, it is necessary to try to keep gas bubble sizes small.

Gas bubbles coalesce naturally when moving upwards through a fluidized bed. When a gas bubble hits a horizontal cylinder in the bed, it is broken up into two or more smaller bubbles that move around the cylinder on both sides.

When using internal heat exchange tubes (which is the case for the PDZ-HF fluidized bed), it is possible to arrange the tubes in a certain configuration to maximise bubble break-up. It was found in laboratory testwork that a staggered configuration of tubes is very effective in bubble break-up (see Figure 2.5).

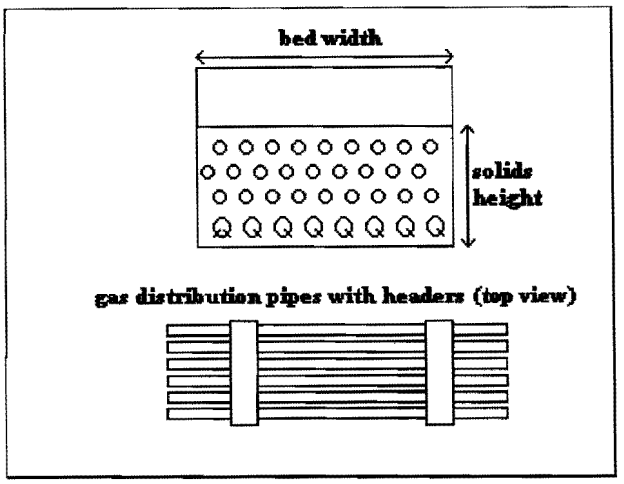

Figure 2.5. Heat exchange tube configuration and gas distribution pipes

The maximum bubble size in the bed is determined by the projected or horizontal distance between two adjacent staggered tubes.

The full-scale perspex model with internal staggered heat exchange tubes demonstrated that the staggered tube configuration was effective for bubble break-up even on the pilot plant scale.

The use of tube banks for heat transfer and bubble break-up in fluidized beds has been studied by Wiman & Almstedt[27], and they found that the tube banks enhance reaction by particle break-up and by inducing an earlier transition to turbulent bed behaviour.

An important consideration pointed out by them is erosion of the tube bank by particle collision. They found that tube bank erosion is less for smaller particle sizes and lower gas velocities. A denser tube bank also reduces erosion.

Grace and Harrison[20] has commented as follows on the use of horizontal tube banks: For high height/diameter ratio's, the use of vertical tube banks are more effective for heat transfer, as the tops and bottoms of the horizontal tubes do not contribute appreciably to heat transfer. For low height/diameter ratio's (as is the case for this application), and when the tubes are used to aid gas distribution, horizontal tube banks can be used.

2.5. Scale-up to commercial scale

It is important that the reaction model used to calculate conversion and yield should fit experimental data well for different operating conditions, and if possible for different reactor sizes. Only then can the reaction model be used with confidence to design a large-scale fluidized bed reactor.

If one wants to observe or inspect the *hydrodynamic* behaviour of a fluidized bed system on a different scale, it is possible to size up or down so that two beds behave hydrodynamically similarly.

The technique to do this was proposed by Fitzgerald and Crane, using the following set of scaling parameters[13]:

$$\frac{d_p u_o \rho_g}{\mu}, \frac{\rho_s}{\rho_g}, \frac{u_o}{(g d_p)^{0.5}}, \frac{h}{d_p} \qquad \textbf{(Eq 2.77)}$$

where the different scaling parameters represent the Reynolds number, the density ratio, the Froude number and geometric similarity, respectively.

For non-catalytic reactions where the reaction rate is fast, scale-up is generally not a problem. Problems occur with catalytic reactions and slow reaction rates. This is because (e.g.) the height/diameter (h/D) ratio does not remain constant with scale-up. Also, solids and gas backmixing in beds with high h/D ratio's is generally considerably less than beds with small h/D ratio's[18]. This leads to reduced contact time and lower conversion and yield.

Careful thought should also go into the design of the bed internals to prevent bubbles from growing much larger than in the lower scale unit and in this way decreasing conversion and yield (because of poorer gas-solid contact).

For these reasons, intermediate scale beds are usually built during scale-up of reactors for slow, catalytic reactions.

A good review of scale-up methodology is given by J.M. Matsen[28].

3. EXPERIMENTAL

3.1. Experimental methods

Initial *reaction kinetic data* for the reaction between gaseous HF and PDZ was obtained from a lab-scale fluidized bed with internal diameter of 100 mm. This unit was also used to evaluate the influence of reaction temperature on achieved conversion.

The *minimum fluidization velocity* in air was determined using a glass column of internal diameter 50 mm, with a porous glass distributor and a manometer for differential pressure measurements.

The effect of *heat exchange tube configuration* on bubble dispersion and break-up was studied qualitatively by utilising a few small rectangular perspex beds with different configurations of internal tubes.

The *upward bubble velocity* in the bed was determined using a two-dimensional perspex bed. A stopwatch and ruler was placed next to the bed and the bed was filmed on video. On video playback it was possible to follow individual bubbles and get time and corresponding distance measurements. Velocities for several bubbles were determined and the average calculated.

The *flow of solids* through a staged bed, with slitted internal baffles, was studied on the full-scale mild steel bed. Only qualitative studies were made, because there was no easy way to put a tracer on some of the particles to try to determine a residence time distribution. The use of colouring was tested in the laboratory and found to be ineffective. The colour meter did not have sufficient resolution to give interpretable results. The use of light particles of different particle size proved ineffective as the particles all shortcutted across the top of the bed. The use of a radioactive tracer would have involved too much safety precautions and legislation to adhere to.

Bubble break-up by the heat exchange tubes was studied on the full-scale perspex bed.

A laboratory-scale perspex *L-valve* was used in a lab fluidized bed system to determine the relationship between gas flow rate to the L-valve and solids flow rate through the L-valve.

3.2. *Analysis methods*

All analyses of samples were carried out by Pelindaba Analytical Labs (PAL), a subdivision of the AEC. The different analyses and methods used are summarised in Table 3.1.

Table 3.1 Analysis methods used

Analysis required	Method used
% Conversion of zircon to PDZ	Gravimetry
% HF in feed liquid	ISE – fluoride Ion Selective Electrode
% Fluoride in product solids	Distillation in HClO, followed by ISE
% Si in solid product (DPDZ)	XRF - X-ray fluorescence
Density, specific surface area	Physical methods
Particle size distribution	Sedigraph – particle size distribution analyser using sedimentation methods.

3.3. *Pilot plant setup*

A process flow diagram of the pilot plant fluidized bed system is shown in Appendix B. This brief process description of the system should be read together with the process flow diagram.

3.3.1 Solids flow

Solids are fed into the system from a feed hopper. The solids flow rate is controlled with a rotary valve or, alternatively, an orifice. From the rotary valve the solids fall into the preheater, which is a single stage fluidized bed.

In the preheater, the solids are heated up to a temperature of 120 °C by fluidizing them with heated air. The solids need preheating to prevent the reaction gas from condensing when coming into contact with cold solids. The air itself is heated by an in-line electric heater. The air exiting the preheater flows through a cyclone where entrained particles are removed and stored in the preheater cyclone hopper.

From the preheater, the solids fall over a weir into a downcomer, where two actuated valves open alternately to let solids through but at the same time provide a positive gas shut-off. The process gas system is run under negative pressure and the preheater system under positive pressure, to ensure that any leakages would be *into* the process gas system.

The two actuated valves feed the solids into the top stage of the fluidized bed reactor, where it is fluidized by a gas mixture of HF and water. The top stage of the fluidized bed serves as the first reactor stage and also catches most of the unreacted HF from the bottom stage, thus improving HF consumption efficiency.

From the top stage the solids is fed through a L-valve into the bottom reactor stage. The bottom reactor stage is divided into four subsections of decreasing cross-sectional area, using internal baffles. The reactor thus has five reactor stages in total.

Both reactor stages use distribution pipes as a distributor, and have internal heat exchange tubes along the length of the rectangular reactor. These heat exchange tubes remove heat generated by the heat of reaction and control the reactor temperature at 120 °C.

Every stage in the reactor has a sampling setup to facilitate the taking of samples during operation.

After the last reactor stage, the solids flow down a downcomer into the product hopper.

3.3.2 Gas flow

A liquid mixture of HF, water and H_2SiF_6 (or alternately only HF and water) is evaporated in a falling film evaporator and the gas is then superheated by a few degrees in a double pipe heat exchanger. A condensate catch pot situated just before the gas entrance in the reactor removes possible condensate.

The gas is distributed through the distributor pipes and bubbles through the solids in the bottom reactor stages. It exits the bottom stage through the distributor pipes of the top stage, which are situated directly above the freeboard region of the bottom stages, and then bubbles through the solids in the top reactor stage.

After exiting the top reactor stage, the process gas flows through a cyclone, which removes most of the entrained particles. The gas then flows through a filter baghouse, where the remaining fine particle dust is removed.

The process gas is then treated in a three-scrubber system (two acid scrubbers and one base scrubber) to catch all the condensables (HF, water and H_2SiF_6). The liquid waste stream from the scrubbers is neutralised with lime.

4. DISCUSSION OF RESULTS

Note: Experimental conditions, data and results are reported in tabular form in Appendix C.

4.1. Kinetic model results

4.1.1. Fitting of models to rate data

The single-stage batch fluidized bed models, as developed in Section 2.3.1, were fitted to experimental data obtained from the lab-scale fluidized bed setup. Computer spreadsheets were set up to predict conversion as a function of time for the specific operating conditions of the experimental data.

The method of least squares was used to determine the best fit for each model and the resulting reaction rate constant.

Figure 4.1 shows the best fit results for the various models.

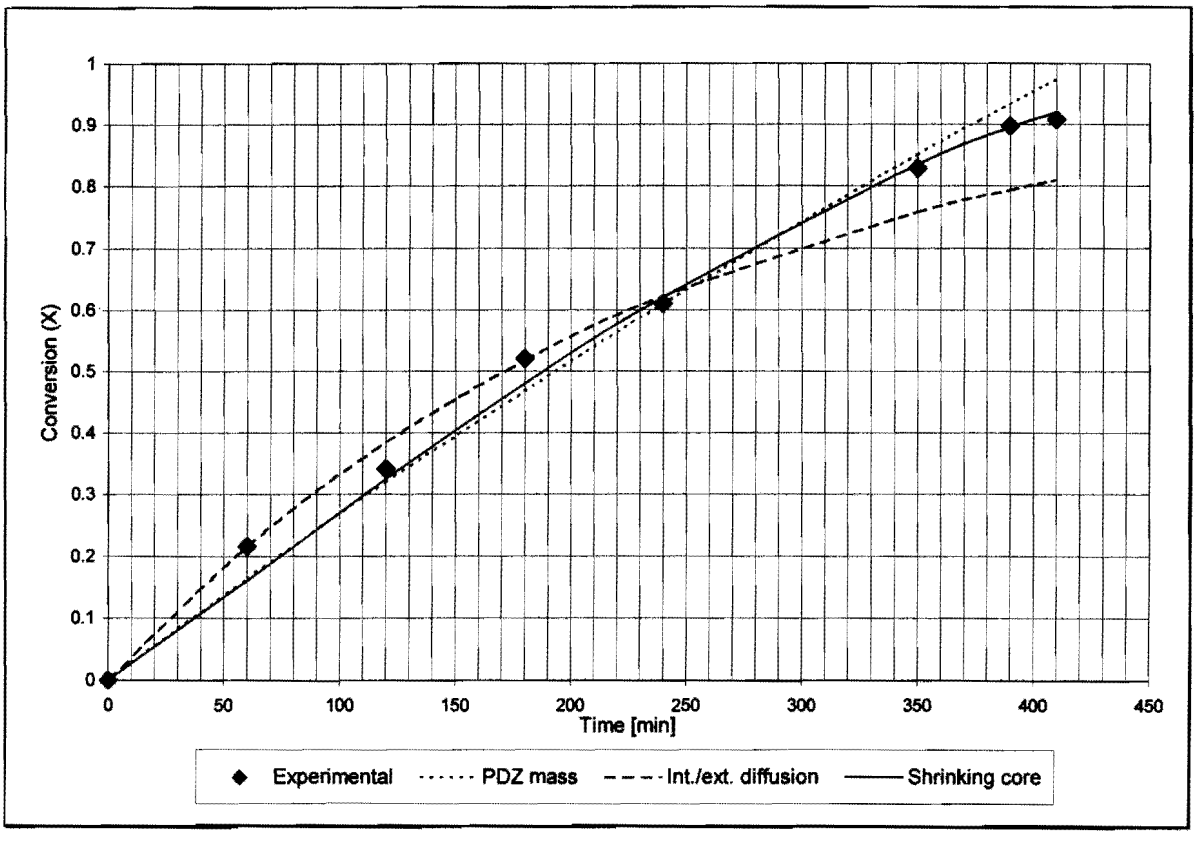

Figure 4.1 Shrinking core model best fits lab experimental kinetic data

The shrinking core model yielded the best results, with an average error of 5.3%. The rate constant for the shrinking core model, as defined in Equation 2.21, is k_s = 6.1E-6 m/s.

4.1.2. Effect of variation of parameters

4.1.2.1. HF gas flow rate

The effect of the HF gas flow rate on conversion time was investigated using the fitted shrinking core model. The reaction conditions from the lab scale fluidized bed was used for this investigation.

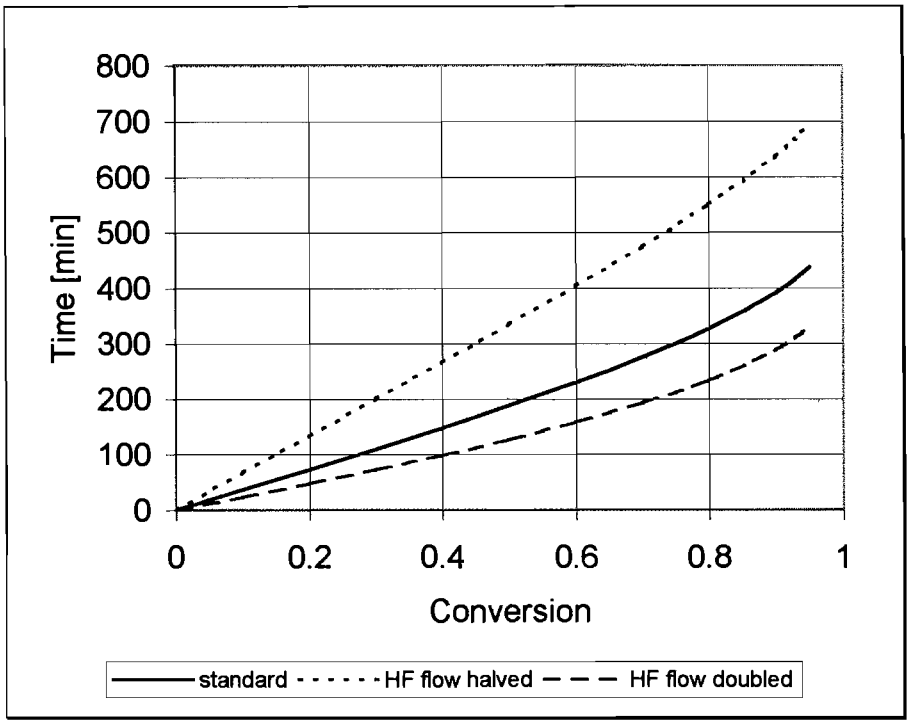

Figure 4.2 Increased gas flow rate can reduce conversion time

As can be seen from Figure 4.2, a reduction in the solids residence time (for equal conversion) can be achieved by increasing the HF gas flow rate through the bed. It should be mentioned that the HF consumption efficiency is negatively influenced by an increase in gas flow rate for a single-stage bed.

For the multi-stage fluidized bed, where the top stage serves as a HF "scrubber", faster HF (or gas) flow rates will reduce bed loads. It will also increase entrainment from the bed. Thus a superficial gas velocity must be chosen to balance the objectives of minimum bed load, minimum entrainment and minimum HF loss (or maximum HF consumption efficiency).

4.1.2.2. Accuracy of rate constant

The dependence of the model on the accuracy of the value of the rate constant was investigated using the shrinking core model. As can be clearly seen from Figure 4.3, the model has a low sensitivity to inaccuracy of the rate constant. For a doubling in value of the rate constant, the reduction in required residence time is low at low conversions.

It is only when very high conversions are required that the rate constant has a big influence on residence time – at 80% required conversion, the difference in residence time is 51 mins (18%), and at 99.5% conversion the time difference is 133 mins (33%).

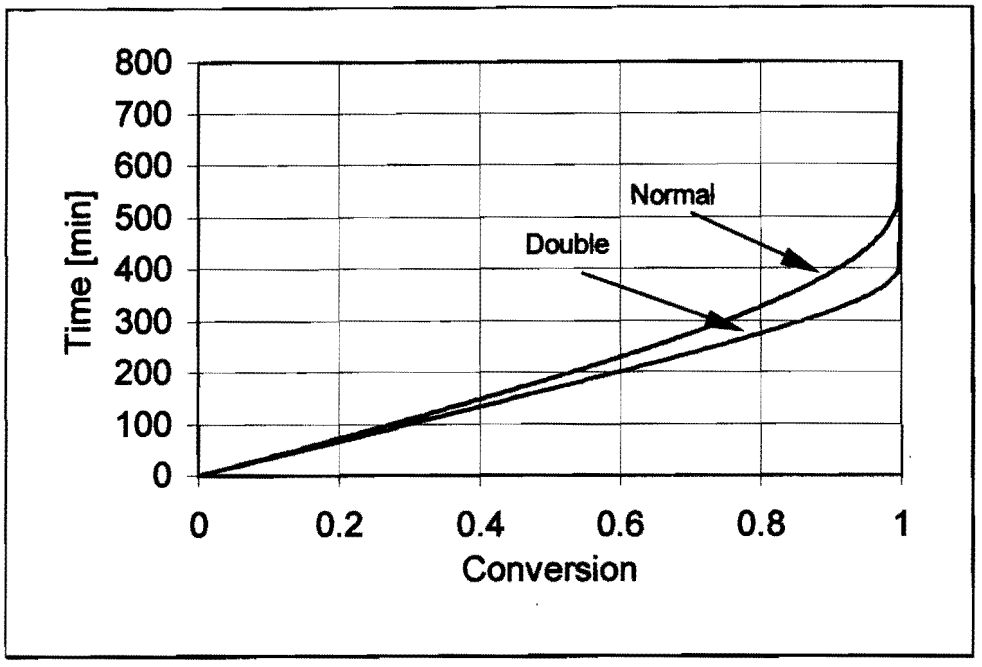

Figure 4.3 Accuracy of rate constant has little influence on reaction rates

4.2. *Fluidized bed modelling results*

4.2.1. Hydrodynamic results

4.2.1.1. Minimum fluidization velocity

The minimum fluidization velocity was calculated from theory, and also determined in different lab setups. The value from the pilot plant was somewhat different from the other values as shown in Table 4.1. All values were determined for air and PDZ at room temperature.

Table 4.1 Minimum fluidization velocity

Calculated (theoretical)	*Lab glass column*	*Lab perspex column*	*Pilot plant (both preheater and reactor)*
2.7 cm/s	2.2 – 2.6 cm/s	2.6 cm/s	1.1 cm/s

The reason for the decrease in minimum fluidization velocity from lab to pilot plant scale could be the reduction of wall effects with increase in cross-sectional area, as the lab experiments were done on very small diameter columns (50 mm).

Another possible reason is the influence of the gas distribution pipes and the heat exchange tube bank, which is distributed over the entire bed height. The effect of these internals is a reduction in the effective cross-sectional area for gas flow. As the minimum fluidization velocity for the pilot plant reactor was calculated using the empty bed cross-sectional area, it

is possible that the actual minimum fluidization velocity is higher because of the reduced effective cross-sectional area. This effect should be kept in mind when designing the commercial scale reactor.

The heat exchange tubes with OD 17 mm are arranged in a staggered configuration with 14 mm horizontal space between two adjacent tubes. If one thus assumes that the actual cross-sectional area of the bed is halved, the minimum fluidization velocity for the pilot plant is 2.2 cm/s, which is much closer to laboratory and calculated values.

4.2.1.2. Pressure drop over distributor pipes

The pressure drop over the distributor pipes as calculated, compares well with the results from the pilot plant (see Figure 4.4), although it appears that the model predicts pressure drops that are too low at higher flow rates and could become inaccurate at very high flow rates.

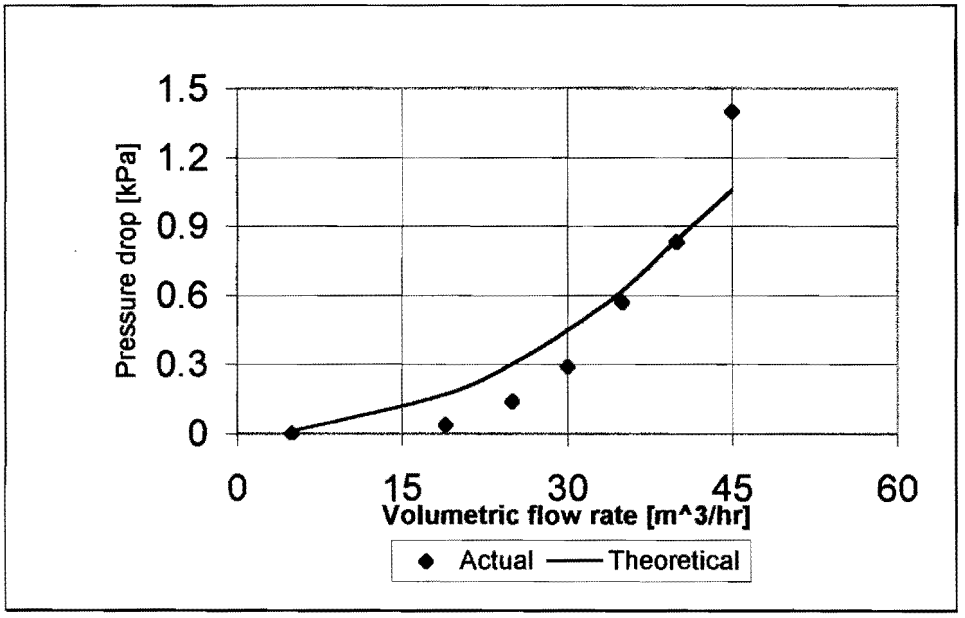

Figure 4.4. Theory predicts actual pressure drop with reasonable accuracy

4.2.1.3. Pressure drop over bed

The theoretical pressure drop at minimum fluidization is given by:

$$\Delta P_b = (1 - \varepsilon_{mf})(\rho_s - \rho_g)gh_{mf}$$

$$\Delta P_b = (1 - 0.45)(2200 - 1.5) * 9.81 * 0.22$$

$$\Delta P_b = 2.6kPa$$

Figure 4.5 shows that the theoretical calculation is reasonably accurate in predicting pressure drop (2.6 vs. 2.9 kPa).

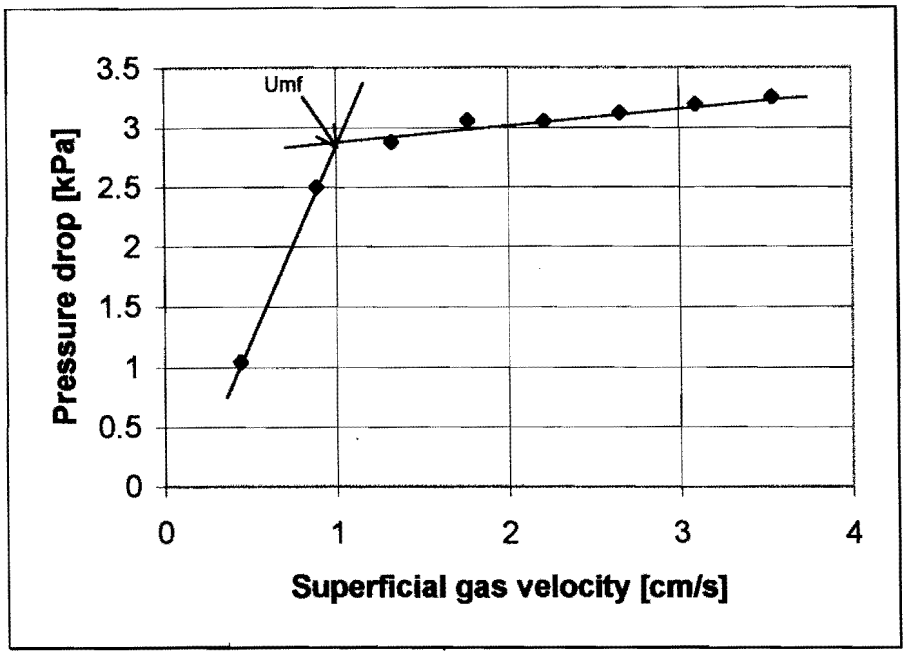

Figure 4.5. Determination of min. fluidization velocity and pressure drop at u_{mf}

4.2.1.4. Influence of mass loss on gas flow distribution

The effect of mass loss on the gas flow distribution in the different substages of the cross-current bed was investigated, as discussed in Section 2.4.1. The results are shown in Table 4.2.

Table 4.2. Influence of mass loss on gas flow distribution.

Substage	1	2	3	4
Conversion (X)	0.631	0.849	0.958	0.994
Vol. Flow [m^3/hr]	**33.0**	**24.4**	**16.1**	**8.0**
Vol. Flow with mass loss [m^3/hr]	**27.64**	**25.76**	**18.59**	**9.52**
Percentage difference [%]	-16.2	5.6	15.4	18.9

From Table 4.2 it can be seen that the effect of the mass loss on gas flow distribution was less than 20% for each of the streams, and the total calculated difference in conversion was less than 0.5% (this was calculated by insertion of the calculated volumetric flow rates in the reaction kinetic model). It was felt that this was small enough to be neglected.

4.2.2. Optimisation of PDZ conversion and HF consumption efficiency

All the calculations on conversion, bed loads, etc. were done with all other operating parameters constant. The values of the constant parameters were typical operating values for the 200 metric ton/year pilot plant.

A point worth mentioning is that the laboratory reactor used anhydrous HF mixed with nitrogen gas as reaction gas. The pilot plant reactor uses a mixture of HF and water (steam) as reaction gas. From this it can be concluded that the influence of these other gases on the

HF-PDZ reaction is not significant, as there was no major change in the kinetic behaviour of the system.

The notation of the graphs and text in this section are as follows:

CC = countercurrent fluidized bed reactor

CRC = cross-/countercurrent fluidized bed reactor with two main countercurrent stages and the second (or bottom) countercurrent stage divided into a number of crosscurrent stages.

ST = total number of stages

Example: 5 st, crc = A combination fluidized bed with two main counter-current stages, and the bottom stage divided into four crosscurrent stages (thus a total of five stages).

4.2.2.1. Bed loads and conversion

Figure 4.6 shows a comparison between total conversion for reactors with different configurations at equal total bed load.

A clarification of the distribution of the equal total bed load is appropriate. An example is given for 200 kg total bed load:

- The three stage CC unit has three stages with bed loads of 66 kg each.
- The five stage CRC unit has two main stages with 100 kg each, and the second main stage has four substages with 25 kg each.
- The six stage CRC unit has two main stages with 100 kg each, and the second main stage has five substages with 20 kg each.

The advantage in terms of bed load (and thus reactor size and solids residence time) of the CRC setup over the conventional CC setup is very evident. A very large reduction in bed volume can be achieved by using the CRC setup.

Figure 4.7 shows a comparison between a 5 stage and 6 stage CRC setup, again with equal bed loads. At lower bed loads, there is a significant difference between the two setups, the 6 stage setup yielding higher conversions for equal bed load. At higher bed loads, the advantage of the 6 stage setup diminishes.

For high conversions (>99%), the required bed loads are approximately equal. Because a reactor with fewer stages is easier to construct, and the desired conversion on the fluidized bed was above 99%, it was decided to use the 5 stage CRC setup for the pilot plant fluidized bed.

UNIVERSITEIT VAN PRETORIA
UNIVERSITY OF PRETORIA
YUNIBESITHI YA PRETORIA

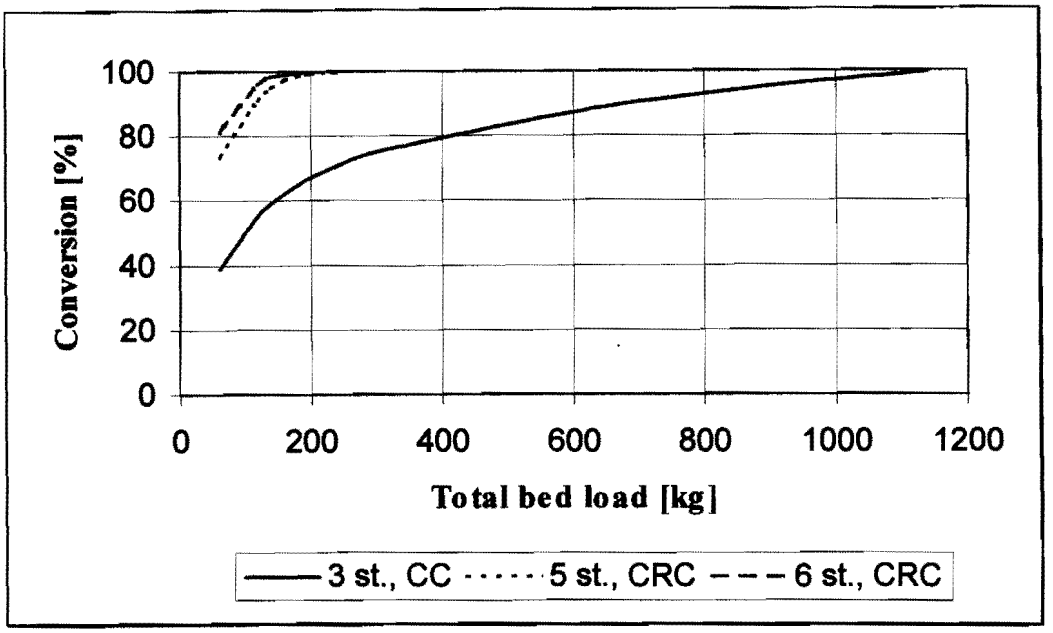

Figure 4.6 CRC units yield large reduction in reactor volume for equal conversion

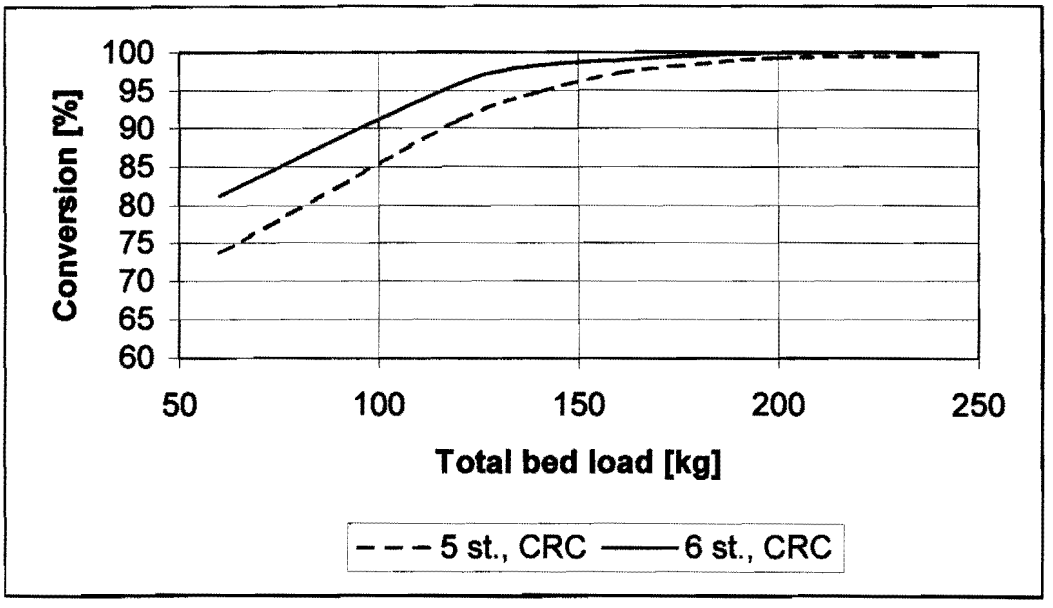

Figure 4.7 Difference between 5 and 6 stage CRC units becomes smaller with increasing bed load

It must be kept in mind that the 5 and 6 stage CRC units actually have 2 countercurrent stages each, compared to the 3 stage CC unit with 3 countercurrent stages. Thus construction of the CRC units are actually simpler than the CC unit, as the crosscurrent staging is achieved by insertion of internal baffles.

The above comparisons were all based on equal bed load distribution between stages. Of course the bed load distribution between the two main stages and between the substages of the second main stage (of the 5 stage CRC unit) can also be varied. Several permutations were investigated to determine the optimum configuration in terms of bed load and HF consumption efficiency.

Some of the optimum distributions are shown in Figure 4.8 for a 5 stage CRC reactor with a total bed load of 200 kg. A comparison is made between the conversions achieved for the same total bed load, but with the load distributed in different ways between the substages (this is achieved by varying the cross-sectional area's of the substages with constant total cross-sectional area).

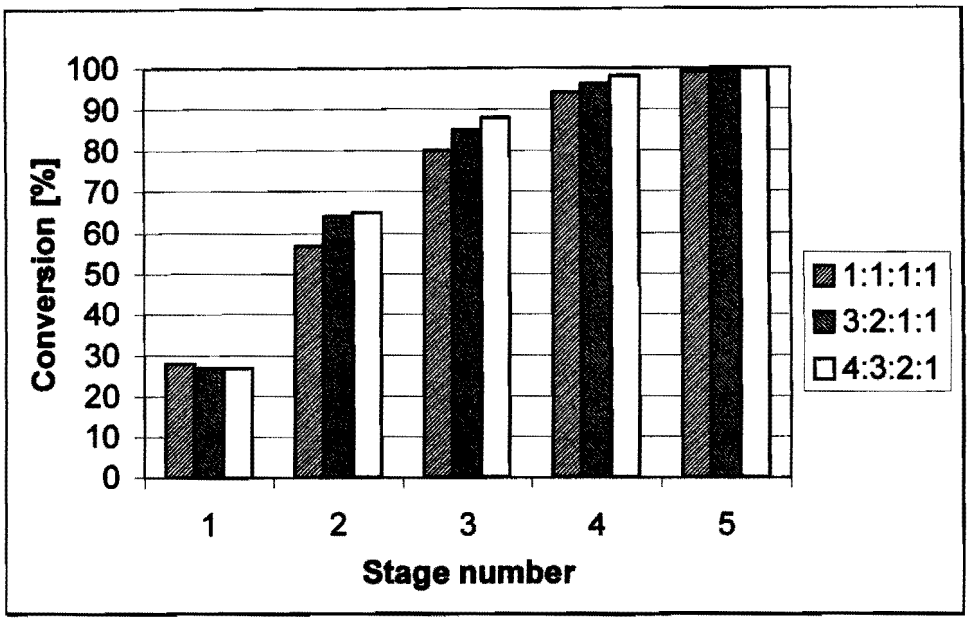

Figure 4.8 Diminishing cross-sectional area substages yield better conversion

As can be seen from Figure 4.8, the configuration with the second main stage divided into substages of diminishing cross-sectional area (4:3:2:1) yielded the best total conversion for equal bed load. It also yielded the highest HF consumption efficiency of 92.6%. This reactor configuration was chosen as the final design configuration for the pilot plant reactor and the total bed load was increased to 240 kg to build in a safety factor.

4.2.2.2. Influence of gas mixing

As discussed in Section 2.3.3, the influence of gas mixing on the overall conversion in the 5 stage CRC fluidized bed reactor was investigated, using the model developed in Section 2.3.3. This model assumed no gas mixing between main stages, and the investigation was carried out to determine the other limit of operation, as the model used in the design of the reactor assumed total gas mixing between main reactor stages.

Figure 4.10 shows a comparison between the two extremes of gas mixing (no mixing and total mixing). For the assumption of no gas mixing it was necessary to break down the first or top main stage into four substages (to correspond with the second or bottom main stage) and the comparison is made on this basis.

Thus there is a total number of eight stages, and the conversion in the top stage for the total gas mixing model corresponds to the conversion in the fourth stage of the no gas mixing model (see Figure 4.9 and Figure 2.3). The cross-sectional areas of the four substages of the top main stage correspond with the cross-sectional areas of the respective substages of the bottom main stage.

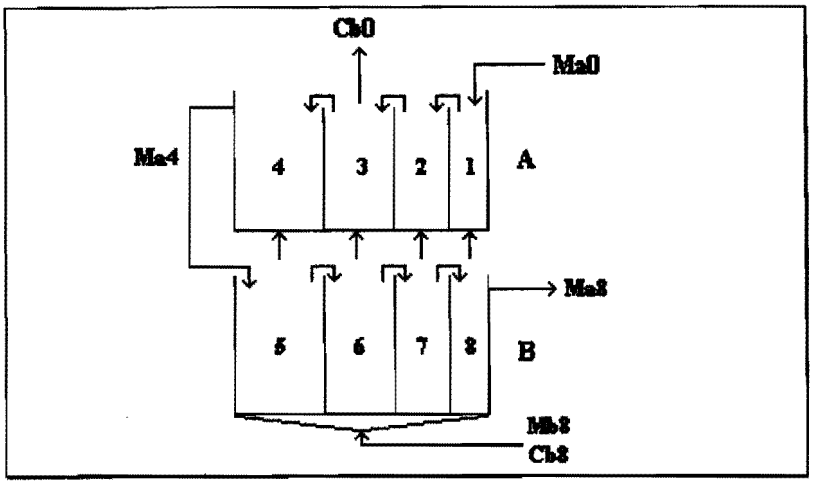

Figure 4.9 Reactor configuration for the no gas mixing model

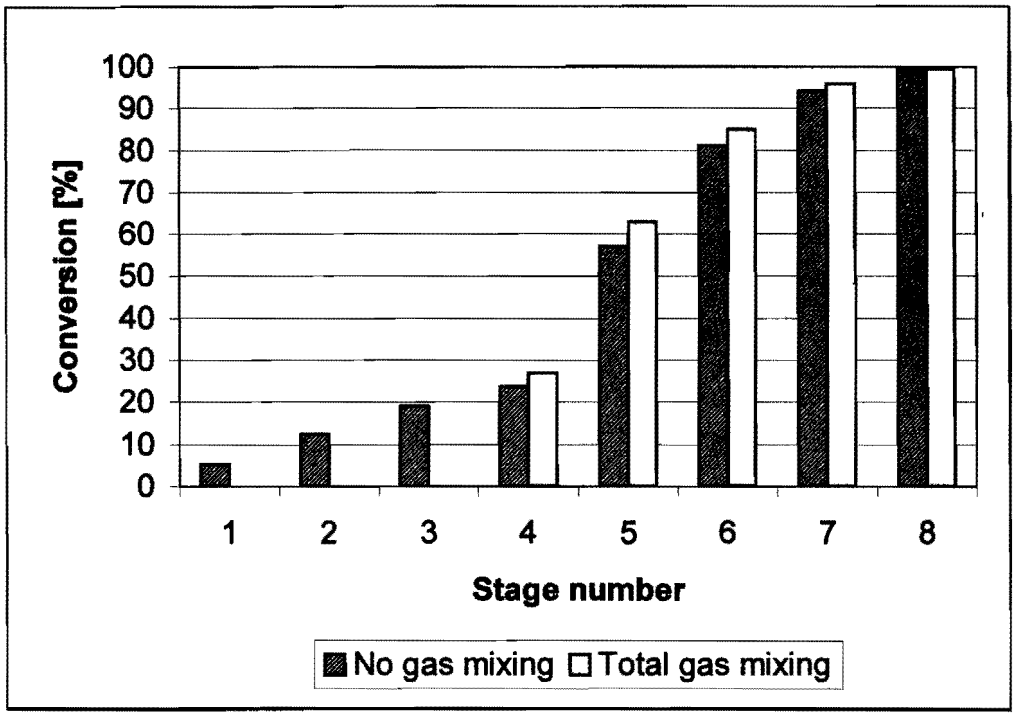

Figure 4.10. Choice of gas mixing model has a negligible effect on final conversion

The model yielded a somewhat lower conversion for the top reactor stage (stage 4 – 24% vs. 27%), but the overall conversion was still higher than 99%. Thus it was concluded that gas mixing effects would not influence reactor performance significantly.

4.3. Comparison of pilot plant results with model

The pilot plant fluidized bed reactor regularly yielded higher than 99% conversion for the design operating parameters. While this excellent reactor performance could be attributed to overdesign, the fact that the predicted batch and steady state profiles correlate so well with the pilot plant profiles (see below), proves that the model was very successful in modelling the real situation.

The CRC reactor configuration was illustrated to be successful in yielding high conversions for relatively low reactor loads (and thus residence times) on a 200 metric tonnes/year scale, as predicted by the model.

Figure 4.11 shows the steady-state conversion profile achieved in the pilot plant reactor compared with the predicted conversion profile from the reactor model. The two profiles show excellent correlation.

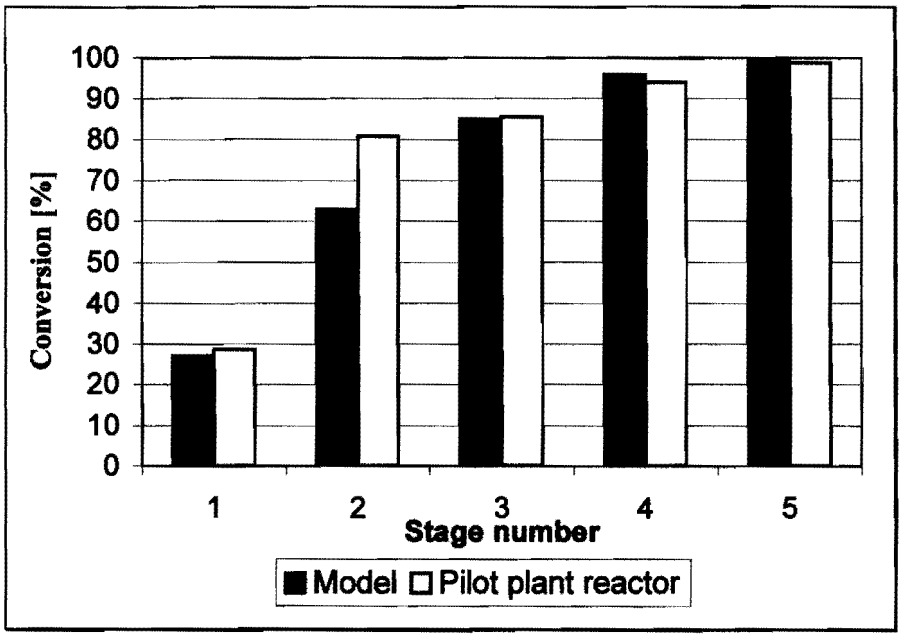

Figure 4.11. Good agreement between steady-state conversion profiles from the model and the pilot plant reactor

In Figure 4.12, a comparison is made between the batch conversion profile obtained experimentally on the pilot plant reactor and the profile calculated using the reaction kinetic model with the pilot plant operating parameters and using the rate constant determined from laboratory data.

It is apparent that the predicted conversion from the model is almost identical to that achieved on the pilot plant reactor. In fact, polynomial curve fitting of the two data sets yields indistinguishable curves. This result is further proof of the validity of the model.

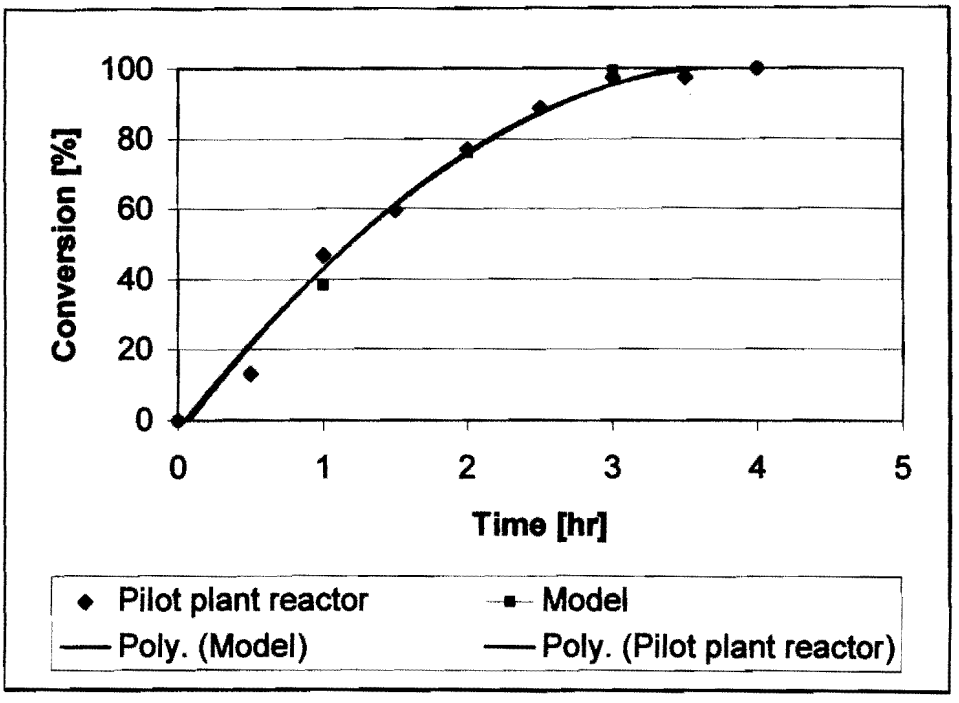

Figure 4.12. Batch reaction rate data from the model show good agreement with data from the pilot plant

5. CONCLUSIONS

5.1. Kinetic model

The developed reaction kinetic model was very successful in predicting conversion for a fluidized bed scaled up by a factor of 10. This success in predicting conversion on different scales with different operating parameters and hydrodynamic behaviour confirms the validity of the model chosen to describe the gas-solid reaction.

Thus it can reasonably be assumed that a shrinking core of PDZ within a porous matrix of zirconia, with reaction as the rate-limiting step and PDZ surface area as solids driving force, is an adequate description of the gas-solid reaction between gaseous HF and PDZ.

5.2. Fluidized bed design

From the reactor model developed using the reaction kinetic model, it was apparent that very large reductions in reactor size could be achieved utilising the CRC reactor configuration, as opposed to the conventional CC reactor configuration.

This model result was confirmed by the fact that the pilot plant reactor, designed from the model, performed as predicted. The pilot plant performance showed excellent correlation with predicted performance.

Thus it can be concluded that different reactor configurations should be investigated when contemplating the use of a fluidized bed reactor for any gas-solid reaction. Significant savings in capital and operating costs can be achieved by finding the reaction kinetic model that most accurately describes the real situation and by carefully applying this model to different reactor configurations.

The hydrodynamic fluidized bed model compared satisfactorily with the pilot plant experimental results, although the calculation of the minimum fluidization velocity proved to be somewhat off. It is possible that the difference between the calculated and actual values are because of the reduced effective cross-sectional bed area for the pilot plant reactor because of bed internals.

The model developed for the fluidized bed reaction of HF and PDZ fit the experimental data very well for both the bench-scale and pilot-scale beds, and thus one can assume that it could be extended with reasonable confidence to a commercial scale. Some refinements and further testing would increase confidence levels.